Journal of Controlled Release 170 (2013) 83–91

Contents lists available at SciVerse ScienceDirect

Journal of Controlled Release

journal homepage: www.elsevier.com/locate/jconrel

Cell surface clustering of heparan sulfate proteoglycans by amphipathic cell-penetrating peptides does not contribute to uptake

Wouter P.R. Verdurmen [a], Rike Wallbrecher [a], Samuel Schmidt [a], Jos Eilander [a], Petra Bovee-Geurts [a], Susanne Fanghänel [b], Jochen Bürck [c], Parvesh Wadhwani [c], Anne S. Ulrich [b,c], Roland Brock [a,*]

[a] Department of Biochemistry, Nijmegen Centre for Molecular Life Sciences, Radboud University Nijmegen Medical Centre, Post 286, PO Box 9101, 6500 HB Nijmegen, The Netherlands
[b] Karlsruhe Institute of Technology (KIT), Institute for Organic Chemistry and CFN, Fritz-Haber-Weg 6, 76131 Karlsruhe, Germany
[c] KIT, Institute for Biological Interfaces (IBG-2), PO Box 3640, 76021 Karlsruhe, Germany

ARTICLE INFO

Article history:
Received 22 November 2012
Accepted 2 May 2013
Available online 10 May 2013

Keywords:
Cell-penetrating peptide
Drug delivery
Endocytosis
Heparan sulfate proteoglycan
Metabolic labeling
Stereochemistry

ABSTRACT

For arginine-rich cell-penetrating peptides (CPPs), an association with heparan sulfate (HS) chains is considered the first step in the stimulation of uptake for many cells. Much less is known about the role of HS chains in the cell-association and internalization of arginine-free amphipathic CPP such as transportan-10 (TP10). Here, we report that various TP10 analogs differ in their capacity to accumulate on HS-rich plasma membranes in an HS-dependent manner. No accumulation was observed on HS-poor plasma membranes or when HS was removed by enzymatic cleavage. The TP10 analog that strongly clustered on the cell surface, also showed a pronounced capacity to form clusters with HS chains in solution. However, aggregation occurred in a thermodynamically different way compared to the interaction of arginine-rich CPP with HS. To monitor the impact of the peptide on the aggregation of the glycocalyx by time-lapse microscopy, sialic acids were visualized by metabolic labeling using copper-free click chemistry to attach fluorophores to metabolically incorporated azido sugars. Strikingly, a highly enhanced HS-mediated accumulation on the plasma membrane of a particular TP10 analog did not correlate with a better uptake. These findings illustrate that the mode of interaction between cell-penetrating peptides and HS chains has important functional consequences regarding peptide internalization and that there is no direct coupling of interaction, accumulation and uptake.

© 2013 Elsevier B.V. All rights reserved.

1. Introduction

Cell-penetrating peptides (CPPs) are a promising class of molecules that are being applied to shuttle membrane-impermeable cargo into cells. To date, most applications relate to biomedical research. Ultimately, the goal is to apply these molecules for therapeutic purposes. After almost twenty years of investigation, there is now a considerable understanding about the routes CPP may exploit to enter into cells [1,2] and the kind of effects they have on the physiology of the cell [3]. There is a widespread agreement that the route of uptake depends on multiple factors, including the type and concentration of the CPP, the cell-type and the cargo, and that multiple import pathways may be exploited simultaneously [1,4,5]. The most prominent types of CPP that can be distinguished are the arginine-rich CPP and the cationic amphipathic CPP. The TAT-peptide and nonaarginines are important representatives of the first class [6,7]. Transportan and its shorter analog TP10 are members of the second one [8,9]. There is ample evidence that in spite of the physicochemical differences, transportans and the arginine-rich CPP are internalized by endocytosis, even though uptake routes may differ in details [10,11].

In the analysis of molecular interactions leading to peptide uptake, studies in particular have addressed the electrostatic binding to lipids and glycosaminoglycans (GAGs), which are negatively charged sugars with a high abundance on the surface of most cell types [12–14]. One of the most prominent findings that has been obtained from GAG-binding studies is that arginine-rich peptides have submicromolar affinities for heparan sulfate (HS) chains, whereas affinities for lipid membranes are much lower [13]. Indeed, abundant evidence exists for the notion that cationic CPPs have the ability to interact with GAGs in biological systems and that this interaction contributes to uptake [10,15–21].

According to a recent model, the initial interaction with arginine-rich CPP leads to GAG clustering and activation of intracellular signaling cascades, and both processes have been proposed to facilitate CPP uptake [20–22]. Specifically, syndecan-4, was shown to be closely involved in uptake [15]. This protein is a ubiquitously expressed member of the syndecan protein family, which next to glypicans is one of the two main families of membrane-bound HS-carrying proteins [23,24]. But other membrane-associated proteoglycans may be involved as well [20]. The Rho GTPase Rac-1 has been suggested as a critical factor in

* Corresponding author. Tel.: +31 24 36 66213; fax: +31 24 36 164 13.
E-mail address: R.Brock@ncmls.ru.nl (R. Brock).

0168-3659/$ – see front matter © 2013 Elsevier B.V. All rights reserved.
http://dx.doi.org/10.1016/j.jconrel.2013.05.001

peptide internalization [20]. Interestingly, highly similar mechanisms have been described for, amongst others, growth factors [25], nonviral delivery systems [26–28], viruses [29,30], and bacteria [31]. These examples suggest that the exploitation of membrane-associated proteoglycans, and in particular syndecans, is a mechanism widely associated with cellular internalization. Additionally, HS chains have been reported to contribute to the uptake of guanidinium-rich CPP mimics [32,33]. For $S4_{13}$-PV peptides HS on the cell surface was required for particle formation [34]. For complexes between DNA and the more hydrophobic MPG-β, HS was required for the induction of lamellipodia formation and for a Rac-dependent cytoskeletal reorganization, associated with uptake [35].

In the analysis of HS clustering, the introduction of fluorescent reporter groups is a challenge. So far, studies have either employed fluorescent fusion proteins of syndecans [15] or immunofluorescent labeling [36]. However, C-terminal fusions of syndecans abolish their PDZ motif and may therefore impair interactions of the cytoplasmic domain while immunofluorescent labeling of the extracellular domain or sugars may affect HS dynamics through cross-linking. Recently, metabolic labeling has been introduced as a powerful approach in chemical biology to introduce sugars for bioorthogonal labeling [37,38]. However, in CPP research, this is a novelty. Cells are cultured in the presence of cell-permeable sugar esters carrying azido-functionalities. Inside the cells, the ester groups are cleaved off through the action of esterases and the sugars with the azido functionalities are incorporated into glycans analogous to the non azido-functionalized endogenous counterparts. After trafficking to the cell surface, labels can be introduced through copper-free click chemistry [39].

Here, we show for transportan-10 (TP10) and a set of TP10 analogs that these CPPs also interact with heparan sulfates on the cell surface but that this interaction is thermodynamically and functionally different from the one described for arginine-rich CPP. Metabolic labeling of sialic acids was employed for the introduction of fluorescent reporter groups in the glycocalyx and for monitoring the colocalization of peptide and sugar clustering on the cell surface. Significantly, the results indicate that HS chains have the capacity to sequester amphipathic CPP in a manner that is unproductive for uptake.

2. Material and methods

2.1. Cell culture

HeLa and Jurkat E6.1 cells were maintained in DMEM and RPMI 1640 (Gibco, Invitrogen, Eugene, U.S.A.), respectively, supplemented with 10% fetal calf serum (FCS; PAN Biotech). All cells were incubated at 37 °C in a 5% CO_2-containing, humidified incubator. Cells were passaged every 2 to 3 days.

2.2. Solid-phase peptide synthesis

All peptides were synthesized on an automated Syro II multiple peptide synthesizer (MultiSynTech, Witten, Germany) with standard Fmoc protocols and HOBt/HBTU as coupling reagents. The unnatural amino acid CF_3-Bpg was coupled manually for 2 h using diisopropylcarbodiimide (DIC) and HOBt. Peptides were N-terminally labeled with 5(6)-carboxyfluorescein before cleavage off the resin and side chain deprotection. For fluorescein labeling, a 5-fold molar excess of 5(6)-carboxyfluorescein:DIC:HOBt (1:1:1) in dimethylformamide (DMF) was added to the peptide on the resin and was allowed to react for 12 h at room temperature. After washing with DMF, dichloromethane (DCM), methanol (MeOH) and diethyl ether, piperidine (20% v/v in DMF) was added for 30 min. Afterwards the resin was washed with DMF, DCM and MeOH, dried under reduced pressure and the peptide cleaved off the resin using a mixture of trifluoroacetic acid (TFA) (93.5%), triisopropylsilane (TIS, 4%) and H_2O (2.5%). The filtrate was evaporated under a gentle stream of N_2 and the crude peptide was precipitated using diethyl ether and lyophilized. The crude peptides were purified by high-performance liquid chromatography (HPLC) on a preparative C18 column (22 × 250 mm) (Vydac, Hesperia, CA, USA) using water-acetonitrile gradients supplemented with 5 mM HCl. The identity of all peptides was confirmed by mass spectrometry. The purity of the peptides was found to be over 95%. The concentration of fluorescein-labeled peptides was determined by measuring A_{492} in Tris–HCl buffer (pH 8.8), assuming a molar extinction coefficient of 75,000 M^{-1} cm^{-1}.

2.3. Bioorthogonal labeling of cells

HeLa cells (40,000 cells/well) were seeded one day before the experiment in 8-well microscopy chambers (Nunc, Wiesbaden, Germany) and incubated in the absence or presence of Ac4ManNAz (50 μM) [38,39] over night. For live-cell labeling, adhered cells were washed three times with HBS and incubated with BCN-biotin (60 μM, SynAffix, Nijmegen, The Netherlands) [40] or buffer (1 h, 20 °C), washed three times with HBS and incubated with HBS containing Alexa Fluor 647-conjugated streptavidin (5 μg/ml, Invitrogen). After incubation (30 min, 4 °C), cells were washed three times and kept in pre-warmed culture-medium for 1 h at 37 °C, 5% CO_2 before treatment with CPPs and confocal microscopy studies.

2.4. Imaging of peptide uptake by confocal microscopy

HeLa cells were seeded one (40,000 cells/well), two (20,000 cells/well) or three (10,000 cells/well) days before the experiment in 8-well microscopy chambers and grown to 75% confluence. Cells were incubated with the indicated concentrations of peptides for 30 or 60 min at 37 °C, as indicated per experiment. Cells were washed twice after incubation and living cells were analyzed immediately by confocal microscopy using a TCS SP5 confocal microscope (Leica Microsystems, Mannheim, Germany) equipped with an HCX PL APO 63× N.A. 1.2 water immersion lens. Cells were maintained at 37 °C on a temperature-controlled microscope stage. Annexin V-Alexa Fluor 647 was used at a dilution of 1:50 (Invitrogen). For heparan sulfate removal HeLa cells were pre-incubated with 3 mIU of heparinase III (Ibex, Quebec, Canada) in DMEM containing 1% FCS for 1 h at 37 °C. For time-lapse confocal microscopy, cell culture medium was replaced by pre-warmed culture medium including 10% FCS, containing TP10 or TP10 Gly2 → *L*-CF_3-Bpg in a final concentration of 5 μM, followed by life cell confocal imaging at 37 °C using excitation at 488 nm and detection of fluorescence over 500–550 nm (fluorescein) and additional excitation at 633 nm and emission of detection over 650–750 nm (BCN-biotin/Streptavidin Alexa Fluor 647 labeled sialic acids) over a timespan of 30 min.

2.5. Flow cytometry

HeLa cells were seeded in 24-well plates (Sarstedt, Numbrecht, Germany) at a density of 80,000 cells/well one day prior to the experiment. Heparinase pre-treatments were performed as described above. Cells were incubated with 5 μM of the indicated peptide for 30 min or 1 h at 37 °C, as indicated. When incubating the peptides at 4 °C, cells were pre-incubated at 4 °C for 10 min to ensure temperature adjustment. Subsequently, cells were washed, detached by trypsinization for 5 min or using a commercial cell-dissociation solution (Merck Millipore, Billerica, USA), spun down and re-suspended in 200 μl RPMI + 10% fetal calf serum in the presence or absence of 0.4% (w/v) trypan blue. When cells were analyzed with trypan-blue solutions *via* flow cytometry, the high concentration of 0.4% (w/v) ensured that quenching was maintained. Propidium iodide was included at a concentration of 2.5 μg/ml, where indicated. Cellular fluorescence was measured using a FACS-Calibur flow cytometer using the 488 nm line of an argon ion

laser for excitation (BD Biosciences, Erembodegem, Belgium) and the data analyzed with the Summit software (Fort Collins, USA) or FCS Express Version 4 Research Edition (De Novo Software, Los Angeles, CA). Results were based on >4000 cells gated on the basis of forward and sideward scatter.

3. Results

3.1. Membrane association of TP10 analogs in HS-expressing HeLa cells depends on the stereochemistry of the introduced ^{19}F-NMR label

The transportan analog TP10 (AYLLGKINLKALAALAKKIL-NH_2) is a prototype amphipathic CPP that is cationic but free of arginine residues. For a solid-state ^{19}F-NMR based study aimed at investigating the membrane-bound structure of TP10, a series of analogs with substitutions of individual residues by D- or L-enantiomers of trifluoromethylbicyclopent-[1.1.1]-1-ylglycine (CF_3-Bpg) were synthesized (manuscript in preparation; Fig. S1). The two TP10 analogs Gly2 → *L*-CF_3-Bpg (**A-*L*-CF3-Bpg-YLLGKINLKALAALAKKIL-NH2**) and Leu4 → *L*-CF_3-Bpg (**AGY-*L*-CF3-Bpg-LGKINLKALAALAKKIL-NH2**) showed a pronounced membrane staining in HS-expressing HeLa cells that was stronger than the one observed for the wild-type (wt) peptide. The observed membrane staining was similar to what we had observed previously for arginine-rich peptides that were largely or entirely composed of D-amino acids and that had shown a reduced uptake in comparison to their L-amino acid counterparts [18]. To assess whether amino acid chirality played a role in this binding pattern, we compared cell binding and cell uptake in HeLa cells of these two TP10 analogs that had shown a pronounced membrane binding when an *L*-CF_3-Bpg was introduced, with the TP10 analogs that had a *D*-CF_3-Bpg substitution at the same position using confocal microscopy (Fig. 1a). Remarkably, changing the stereochemistry of CF_3-Bpg had a major impact on the membrane staining. Membrane-bound fluorescence was markedly reduced or even absent for the counterparts that had a *D*-CF_3-Bpg substitution. Testing the internalization efficiency by flow cytometry after incubating the cells for 1 h with peptide and quenching of fluorescence associated with the outside of the cell with trypan blue [41–43], we confirmed that most of the visible fluorescence for TP10 Gly2 → *L*-CF_3Bpg represented peptide bound to the extracellular leaflet of the membrane (Fig. 1c). The reduction of fluorescence for TP10 Leu4 → *L*-CF_3-Bpg by trypan blue was significantly lower, despite a considerable membrane staining after 30 min. Thus, it can be concluded that TP10 Leu4 → *L*-CF_3-Bpg showed a higher internalization efficiency, whereas the internalization of all other tested peptides differed only mildly. Also, the strong membrane-staining TP10 Gly2 → *L*-CF_3Bpg analog showed the same internalization efficiency as the wild-type peptide. It should be noted that a proportion of extracellularly bound peptide may have been removed during the trypsinization step, which could lead to an underestimation of the amount of membrane-bound peptide.

Next to the analysis of membrane binding and internalization in HeLa cells, we also investigated the behavior of these TP10 analogs in the suspension Jurkat E6.1 cell line. This cell line serves as a particularly interesting comparison, because it is known not to carry HS chains to any significant degree. Unlike HeLa cells it shows comparable uptake for D- and L-arginine-rich peptides [18]. In order to investigate to which extent HeLa and Jurkat cells also differ with respect to other glycosaminoglycans, we acquired an expression profile using a set of six single-chain antibody fragments with reactivity for epitopes present on chondroitin sulfates, dermatan sulfates and heparan sulfates (Fig. S2). Most epitopes were present in large amounts on HeLa cells, and only marginally on Jurkat cells, thereby confirming their roles as model cell lines expressing high (HeLa) and low (Jurkat) amounts of HS.

If the membrane binding observed in HeLa cells was mediated by HS chains, one would expect that the TP10 analogs Gly2 → *L*-CF_3-Bpg and Leu4 → *L*-CF_3-Bpg would be less enriched at the membrane in Jurkat cells. Indeed, when these cells were incubated for 30 min at

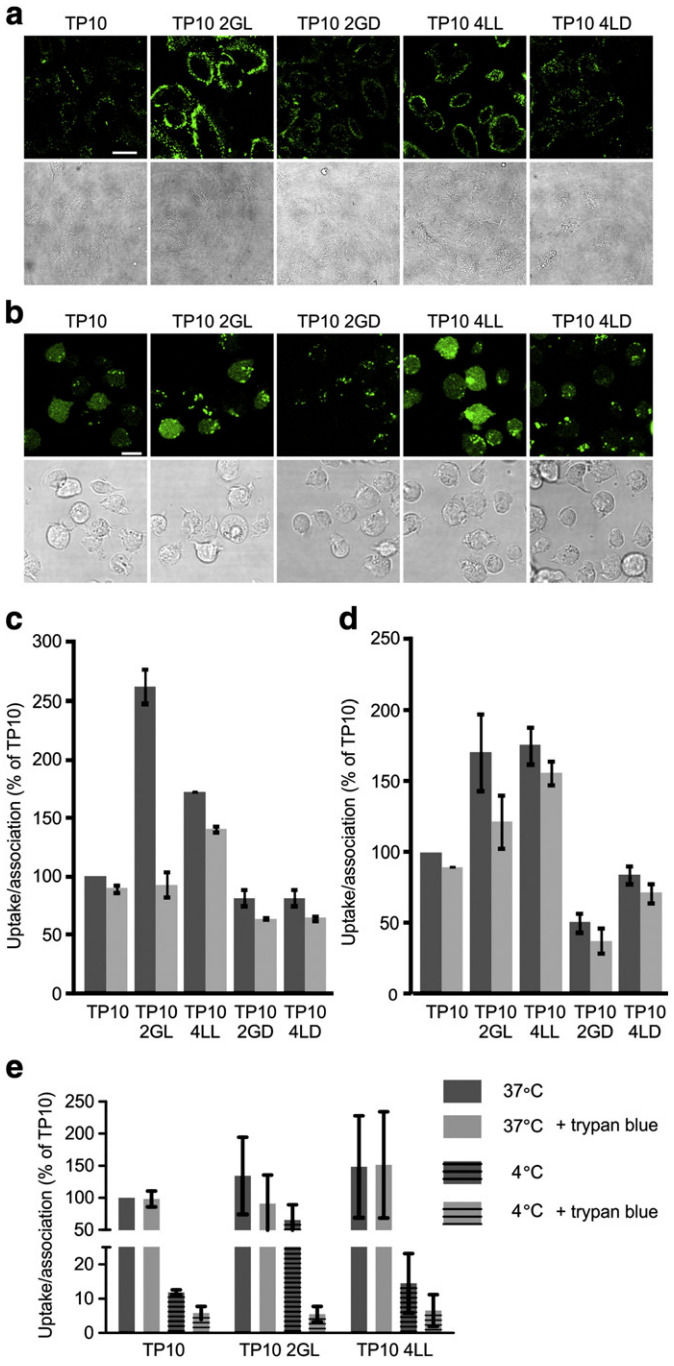


Fig. 1. Cellular association and uptake of TP10 and TP10 analogs with *D*- or *L*-CF_3-Bpg amino acid replacements in HeLa and Jurkat cells. a–b) HeLa (a) and Jurkat (b) cells were incubated with 5 μM of the respective peptides for 30 min at 37 °C, washed and imaged immediately by confocal microscopy. The scale bar corresponds to 20 (a) and 10 μm (b). c–e) HeLa (c) and Jurkat (d, e) cells were incubated for 1 h at 37 °C or additionally at 4 °C (e) in 24-well plates with 5 μM (c, d) or 2.5 μM (e) of the indicated peptide. After washing the cells, cells were detached by trypsinization (only HeLa cells), washed by centrifugation (both cell lines) and resuspended in medium in the presence (light bars) or absence (dark bars) of trypan blue. The error bars represent the range of two independent experiments for which fluorescence was normalized relative to the signal obtained for TP10 without trypan blue. TP10 2GL/D = TP10 Gly2 → *L*/*D*-CF_3-Bpg; TP10 4LL/D = TP10 Leu4 → *L*/*D*-CF_3-Bpg.

5 μM, no generalized membrane binding was evident by confocal microscopy for any of the TP10 analogs (Fig. 1b). Instead, a trend towards a more intense cytoplasmic fluorescence was observed and this cytoplasmic staining was more intense for those peptides that had shown higher membrane binding on HeLa cells. The absence of significant membrane binding of TP10 Gly2 → *L*-CF_3-Bpg was further

confirmed by quantifying the internalization in the absence or presence of trypan blue, which resulted in much smaller differences for this particular peptide than on HeLa cells (Fig. 1d). The differences are also evident from the flow cytometry histograms, which showed a pronounced reduction of signal for TP10 Gly2 → *L*-CF_3-Bpg in HeLa cells when trypan blue was included (Fig. S3b). No such shift was observed for TP10 wt (Fig. S3a) in HeLa cells or in Jurkat cells for either of the two peptides (Fig. S3c,d).

The stronger cytoplasmic fluorescence in Jurkat cells suggested that in comparison to HeLa cells, next to uptake by endocytosis cellular uptake could also occur by direct membrane translocation. To obtain further insight into the mechanism of uptake, cell association and uptake were also assessed at 4 °C for TP10 and two of its analogs, a condition that is generally applied to test for an involvement of energy-dependent endocytosis in uptake. At 4 °C, there was 90–95% reduction of intracellular fluorescence for all peptides consistent with endocytic uptake (Fig. 1e). Remarkably, at 4 °C TP10 Gly2 → *L*-CF_3-Bpg showed a much stronger membrane staining than the other two analogs as deduced from the capacity to quench this signal by trypan blue.

Next, we set out to define whether homogenous cytoplasmic fluorescence represented intact peptide that had escaped the endosomes or fluorescent fragments. For this purpose, cells were incubated with the broad-range cysteine protease inhibitor E64d. Previously, we had established that at concentrations at which the uptake of nona-arginine occurs *via* endocytosis, cytosolic fluorescence could be abolished by a pre-incubation with E64d, which led us to reason that predominantly peptide fragments reach the cytosol, and not intact peptide [18,44]. E64d did not affect the cytoplasmic staining. In combination with the reduction of uptake at 4 °C this result supports the notion that the major part of TP10 and analogs access the cytosol by endosomal escape in an intact form (Fig. S4). This finding is consistent with the fact that TP10 has a higher proteolytic stability against degradation by serum than nonaarginine [45].

3.2. Heparan sulfates and membrane binding

For D-amino acid-containing arginine-rich peptides, we had shown that the enzymatic removal of HS chains strongly reduced the membrane staining [18]. Furthermore, isothermal titration calorimetry (ITC) measurements to study the interaction of these peptides with heparan sulfates gave binding constants in the submicromolar range [18], suggesting that membrane staining was due to binding to heparan sulfates at the cell surface. Since TP10 lacks arginine residues and has a strong propensity to form an amphipathic α-helix [46,47], we expected that TP10 would have a lower affinity for HS chains and perhaps a higher affinity for the lipid bilayer compared to arginine-rich peptides. Therefore, we wanted to directly assess the role of HS chains in the membrane-enrichment of the TP10 analog Gly2 → L-CF_3-Bpg. For this purpose, heparan sulfates were enzymatically digested off the surface of HeLa cells (Fig. 2a). To assess in more detail whether heparinase III cleaved off the chains efficiently, we also analyzed the GAG profile after heparinase III treatment using three anti-HS antibodies, which showed indeed a reduction of over 90% for all three epitopes (Fig. S2).

To make sure that heparinase did not modify the overall structure of the plasma membrane or the capacity of lipophilic compounds to insert into the lipid bilayer, the plasma membrane stain CellMask was included as a control after the heparinase treatment. The distribution and intensity for CellMask were not changed after the treatment. In contrast, the heparinase treatment strongly reduced the intensity of the membrane staining of TP10 Gly2 → *L*-CF_3-Bpg (Fig. 2a). We then continued to quantify the membrane accumulation and peptide internalization after the heparinase treatment, using a non-enzymatic dissociation solution to detach the cells from the 24-well plate and trypan blue to quench any extracellular peptide. In agreement with the results from confocal microscopy, the heparinase treatment considerably reduced the membrane-associated fraction of TP10 Gly2 → *L*-CF_3-Bpg after

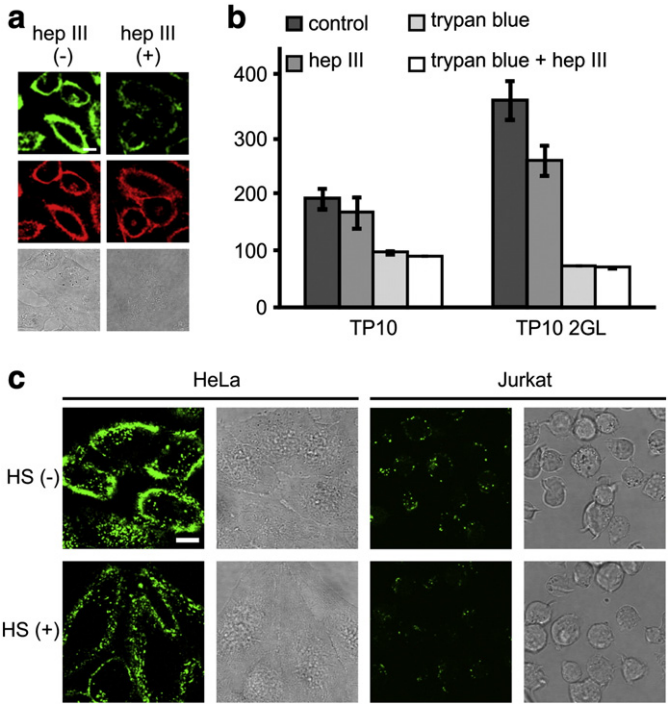


Fig. 2. Role of heparan sulfates in cell association. a) Effect of heparinase treatment on membrane staining of the TP10 analog Gly2 → *L*-CF_3-Bpg (Green: peptide; red: cell mask). The scale bar corresponds to 10 μm. b) Quantification of the effect of a heparinase treatment on the membrane staining of TP10 wt and its analog Gly2 → *L*-CF_3-Bpg. HeLa cells were either treated with heparinase III (hep III) or left untreated, and then incubated for 30 min with 5 μM of the indicated peptide. Cells were detached using an enzyme-free cell-dissociation solution and cell-associated fluorescence was measured in the presence and absence of trypan blue by flow cytometry. c) Effect of competition with externally added HS chains on membrane binding of TP10 Gly2 → *L*-CF_3-Bpg. 2 μM of the peptide were incubated for 30 min at 37 °C in the presence or absence of 5 μM HS. After the incubation, cells were washed twice and imaged immediately by confocal microscopy. The scale bar corresponds to 20 μm.

30 min incubation (Fig. 2b), whereas membrane binding of the wild-type peptide was only mildly affected. Also after 30 min, the enhanced membrane-accumulation of TP10 Gly2 → *L*-CF_3-Bpg did not translate into a greater internalization compared to TP10 wt, as deduced from the cell-associated fluorescence in the presence of trypan blue (Fig. 2b). Heparinase treatment also did not affect the relative or absolute internalization efficiencies of TP10 wt and TP10 Gly2 → *L*-CF_3-Bpg after 30 min incubation. Notably, the relative degree of internalization of TP10 wt as compared to TP10 Gly2 → *L*-CF_3-Bpg was higher for a 30 min incubation period than for a 60 min incubation, but it is unclear whether this indicates different kinetics or whether it reflects saturation, export or degradation characteristics. This was not further addressed in this study. A further confirmation of the role of HS chains was obtained through co-incubating TP10 Gly2 → *L*-CF_3-Bpg with HeLa or Jurkat cells in the presence or absence of HS chains, which abolished membrane-binding in HeLa cells, whereas no major effect was observed in Jurkat cells (Fig 2c).

3.3. Visualization of peptide and sugar clustering using metabolic labeling

The most direct means to demonstrate that clustering of TP10 Gly2 → *L*-CF_3-Bpg is mediated by the presence of HS would be direct time-lapse visualization of peptide and sugar clustering on the cell surface. So far, such studies have mostly relied on the expression of fluorescent fusion proteins of syndecans. However, with the selection of a

particular syndecan, this approach always carries a certain degree of arbitrariness and leads to an overexpression of the selected glycosaminoglycan. In order to monitor the impact of the CPP on the subcellular distribution of the glycocalyx we therefore explored the use of metabolic sugar labeling, an approach that has not been used in drug delivery studies so far. Cells were cultured over night in the presence of peracetylated N-azidoacetyl-mannosamine (Ac4ManNAz) as a metabolic sugar precursor, resulting in the incorporation of azido-containing sialic acids in sialic acid glycoconjugates [38,48]. Once these sugars have reached the cell surface, functional groups can be introduced by copper-free click chemistry (Fig. S5). In this way, it was also possible to follow the effect of HS removal on GAG clustering. Fluorescence was introduced by coupling of a biotin moiety followed by incubation with Alexa Fluor 647-labeled streptavidin. For Hela cells, the labeling protocol resulted in a distinct staining of the entire plasma membrane (Figs. 3, S6, S7). Since this protocol has not been used in the context of CPP delivery, we first assessed the impact of metabolic labeling on peptide uptake. Introduction of the azido-sugar alone had no impact on the uptake of TP10 wt and showed a slight increase (8%) in binding of TP10 Gly2 → *L*-CF_3-Bpg to the cell surface. Labeling with streptavidin had also no impact on binding to the cell surface and uptake for TP10 wt, and again showed just a slight increase (8%) in binding of TP10 2GL to the cell surface but no difference in uptake compared to the untreated control cells. Cells, incubated with R9 showed also an increase (38%) in binding to the cell surface, whereas the uptake was higher (15%/25%) for cells incubated with the azido sugar and additionally incubated with streptavidin, respectively (Fig. S8). Overall these controls demonstrate that the oligovalency of streptavidin had no functional consequences, consistent with previous results on studies on tumor cell morphology and migration, in which metabolically labeled human melanoma cells developed the common mesenchymal phenotype [39].

Time-lapse imaging was performed for TP10 and TP10 Gly2 → *L*-CF_3-Bpg. Due to the presence of fluorescently labeled peptide in the tissue culture medium the membrane accumulation of peptides was less pronounced than in the previous experiments, in which cells had been washed before imaging. For TP10 we only observed an enrichment of peptide in preexisting sugar clusters (Figs. 3, S6). For TP10 Gly2 → *L*-CF_3-Bpg clusters on the plasma membrane appeared over time that colocalized with an enrichment in labeled sugars (Figs. 3, S7). Most importantly, following heparinase treatment, the sialic acid labeling was left intact. However, the heparinase treatment virtually abolished the generation of TP10 Gly2 → *L*-CF_3-Bpg clusters on the plasma membrane.

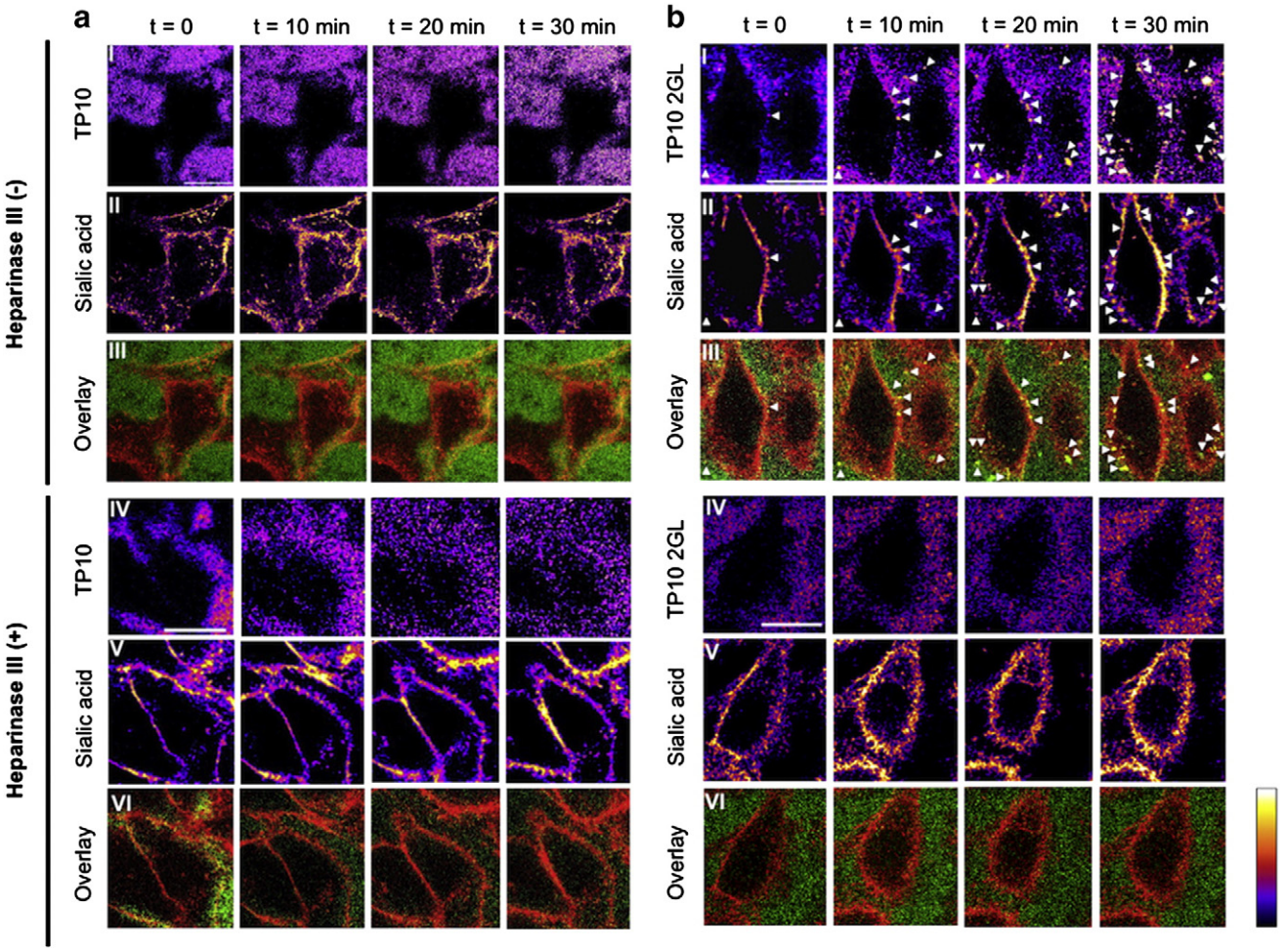


Fig. 3. TP10 Gly2 → *L*-CF_3-Bpg but not TP10 wt induces clustering of HS chains. (a, b) HeLa cells were cultured over night in the presence of Ac4ManNAz (50 μM). Cells were either left untreated (a I–III, b I–III) or treated with heparinase III (a IV–VI, b IV–VI) for 1 h at 37 °C, followed by labeling of incorporated azido sialic acid moieties with a bicyclo[6.1.0] nonyne (BCN)-biotin conjugate and secondary labeling with streptavidin-Alexa Fluor 647. Subsequently, TP10 wt or TP10 2GL was administered in a final concentration of 5 μM, followed by time-lapse confocal microscopy over 30 min at 37 °C. (a) Representative time-lapse confocal images of cells, showing no signs of cluster-formation of the administered TP10 in heparinase III un-treated (a I) and treated (a IV) cells and no apparent changes in the cell surface distribution of sialic acids (a II + V). (b) Time-lapse confocal images of cells, showing the formation of TP10 Gly2 → *L*-CF_3-Bpg clusters (I) accompanied by distinct cluster formation of cell surface sialic acid moieties (II), colocalized with Gly2 → *L*-CF_3-Bpg (III), highlighted by arrowheads. The distinct cluster formation of TP10 Gly2 → *L*-CF_3-Bpg as well as azido sialic acids is abandoned on cells, treated with heparinase III indicating the dependency of cluster formation on the presence of heparan sulfates (IV–VI). The false color look-up table ranges from black (low) to white (high). The scale bar corresponds to 20 μm.

3.4. Biochemical characterization of the interaction of TP10 analogs with HS

To obtain further insight into the nature of the interaction between HS chains and TP10 analogs, we set out to measure the affinity of TP10 wt and the analog TP10 Gly2 → *L*-CF_3-Bpg for HS by isothermal titration calorimetry (ITC). However, using similar conditions that had given submicromolar affinities for D/L-R9 and D/L-penetratin [18], we could not obtain reliable dissociation constants. At 25 °C, no binding enthalpy above background levels could be detected. Only at 37 °C, the HS-TP10 interaction produced a significant change in enthalpy (data not shown). However, it was obvious that the occurrence of massive aggregation (see below) prevented the determination of meaningful K_D values.

In view of the ITC results, we resorted to dynamic light scattering (DLS), a method that would enable the detection and size determination of particles formed between HS and TP10 (analogs). Each TP10 analog, as well as TP10 wt and R9, all fluorescein-labeled, were incubated at a concentration of 5 μM with 10 μM HS. The scattering intensity was measured before and directly after mixing the peptides with HS. Interestingly, the individual analogs varied greatly in the observed increases in scattering intensity in the presence of HS, which reflected differences in the capacity of the TP10 analogs to form aggregates with HS. Prominently, the TP10 analog Gly2 → *L*-CF_3-Bpg, that showed the pronounced aggregation on the plasma membrane of HeLa cells, showed by far the highest increase in scattering intensity (Fig. 4). It should be noted, however, that the scattering intensity is a function of both the size and the number of aggregates. Therefore, this parameter is not suitable to compare exact numbers of aggregates formed. Notably, the clusters that were formed between R9 and HS were considerably smaller than clusters between TP10 Gly2 → *L*-CF_3-Bpg and HS (Fig. S9). The aggregate sizes of the other TP10 analogs were generally closer to the size of those formed with TP10 Gly2 → *L*-CF_3-Bpg. However, aggregate sizes obtained for these other analogs were much more variable, making it difficult to present representative sizes (data not shown). The increased variability may be either due to the relatively low scattering signal or to a slower kinetics of aggregate formation.

The interaction between the TP10 analogs and HS was further investigated by circular dichroism (CD). To eliminate an impact of kinetics on the observed results, all samples were measured after an initial incubation of 30 min at 37 °C at varying HS/peptide ratios (Fig. S10). Surprisingly, all TP10 analogs behaved in a very similar manner in the presence of HS chains. Strongly turbid solutions were obtained when TP10 or its analogs were mixed with HS up to the point of charge neutralization, which resulted in a severe depression of the CD signal due to differential light scattering and absorption flattening artifacts. Addition of more HS, however, led to clear solutions with a restored CD signal intensity. Noticeably, a large excess of HS led to a more pronounced α-helical structure in a comparable manner for all TP10 analogs including the wild type peptide, as is evident from the characteristic CD lineshape with a positive band at 192 nm, and two negative bands around 208 and 222 nm. Mixing HS with R9 did not result in turbid solutions at any HS–peptide ratio. These CD results confirm the observations obtained with dynamic light scattering above, namely that the clusters formed between HS and R9 are generally much smaller compared to clusters between HS and TP10 analogs. Also, no pronounced secondary structure of R9 could be discerned, which is in agreement with previous findings [49].

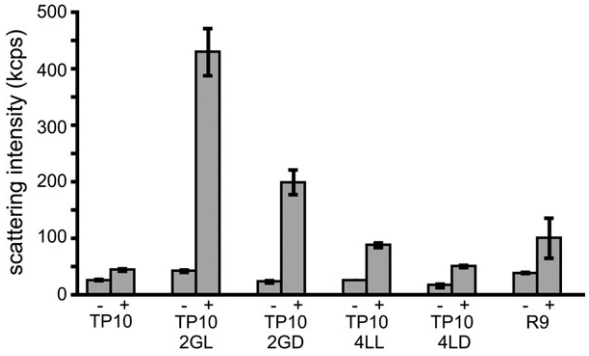


Fig. 4. Scattering intensity of peptide solutions as measured by dynamic light scattering. Peptide solutions were measured in the presence (+) or absence (−) of 10 μM HS chains. Error bars reflect the range of two independent experiments. TP10 2GL/D = TP10 Gly2 → *L*/*D*-CF_3-Bpg; TP10 4LL/D = TP10 Leu4 → *L*/*D*-CF_3-Bpg.

3.5. Induction of phosphatidylserine exposure by TP10

Very evidently for TP10 and its analogs, the interaction with HS chains does not contribute to peptide uptake. Our detailed biochemical analysis showed that TP10 and the arginine-rich peptides engage HS in fundamentally different manners. Finally, we were also interested to learn to which degree the two classes of peptides differed in their interaction with the lipid bilayer. Lipid bilayer remodeling has been repeatedly implicated in various CPP uptake mechanisms, and may in particular play an important role in direct peptide translocation — whereby the peptide directly accesses the cytosol from the extracellular environment [50,51]. Here, we analyzed lipid bilayer organization by measuring to which degree the TP10 analogs and R9 induced phosphatidylserine (PS) exposure. Typically, PS is confined to the inner leaflet of the plasma membrane. Exposure of this phospholipid therefore indicates a disturbance of the lipid bilayer, which may be associated with peptide internalization. In this case a concentration of 25 μM was selected, since the PS-derived signal was expected to be too weak at 5 μM. For arginine-rich peptides at this concentration lipid remodeling through the induction of sphingomyelinase activation occurs. However, the integrity of the plasma membrane barrier function remains preserved [51]. R9 only induces punctuate exposure of PS, in combination with uptake through acid sphingomyelinase-dependent nucleation zones [51,52] (Fig. S11). When HeLa cells were incubated with TP10 at this concentration, already after 4 min a marked difference in PS exposure was observed, which coincided with massive internalization of peptides into the cytoplasm supporting the hypothesis that, although no specific membrane component could be identified in this experiment, the activity of TP10 is much more directed towards the lipid bilayer compared to R9 (Fig. S11). When directly comparing TP10 and TP10 Gly2 → *L*-CF_3-Bpg, also at 25 μM and using identical settings, we found that TP10 Gly2 → *L*-CF_3-Bpg did not affect PS exposure at all. This result indicates that capture of the peptide in the glycocalyx prevented the peptide from disrupting bilayer organization (Fig. 5).

4. Discussion

Even though the field of CPP is moving ever closer to clinical applications, the molecular interactions playing a role in their cellular uptake are still under investigation. For arginine-rich peptides, there is a considerable agreement that the interaction with HS chains on the plasma membrane is an important step in the initiation of internalization. For arginine-free amphipathic peptides such as TP10, however, much less is known about the role of HS in cellular uptake. Here, we show that TP10 analogs, in spite of a much lower affinity, form clusters with HS chains. Average cluster size is much larger than the one observed for nonaarginine. Most significantly, the enhanced aggregation of the TP10 analog Gly2 → *L*-CF_3-Bpg did not translate into an enhanced internalization. This argues that the interaction of cells with this TP10 analog leads to an HS-dependent sequestration of the peptide on the plasma membrane in a manner that is unproductive with respect to peptide internalization. As a novelty in the study of CPP delivery we employed metabolic labeling to assess the impact of peptide binding on the distribution of the glycocalyx.

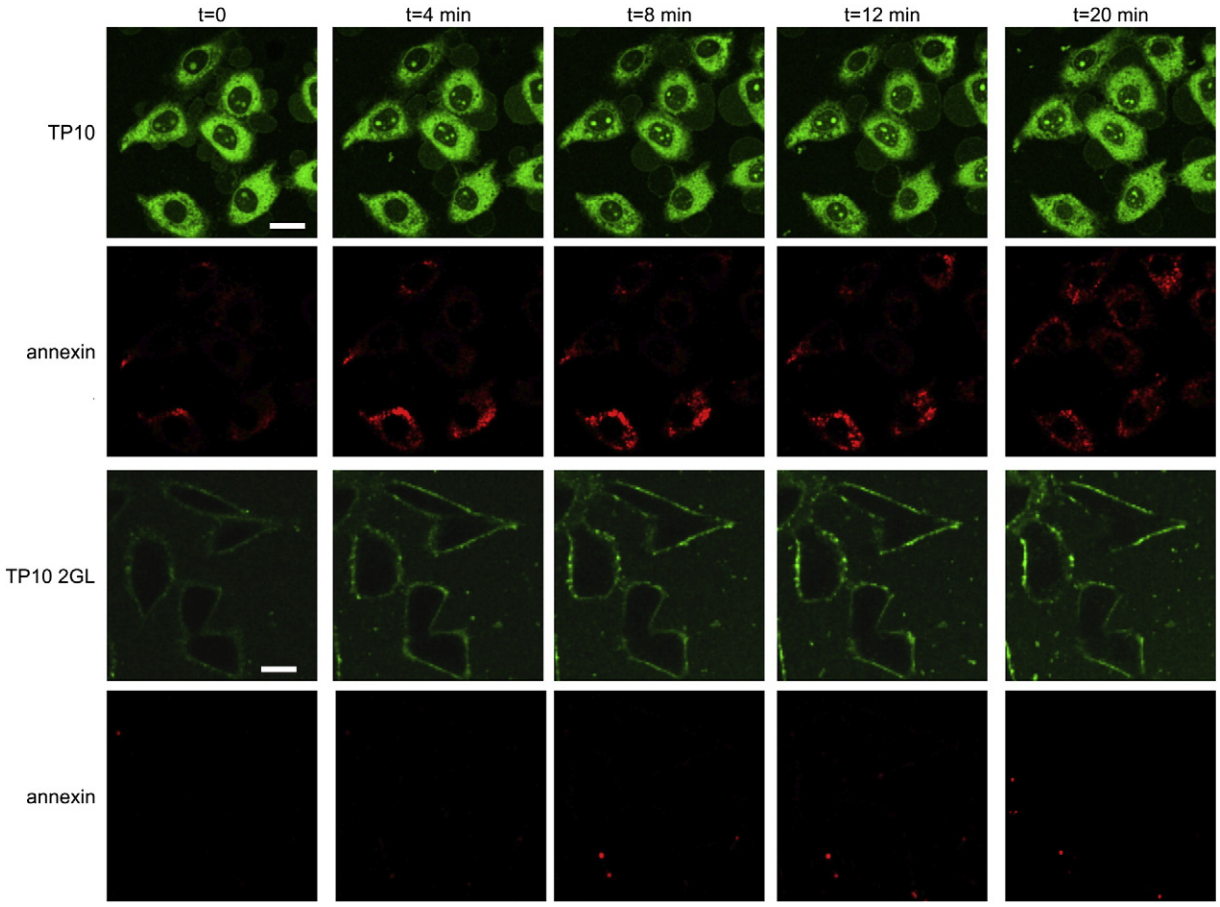


Fig. 5. Induction of PS exposure by TP10 and TP10 Gly2 → *L*-CF_3-Bpg. HeLa cells were co-incubated with 25 μM of the indicated peptides and Annexin V-Alexa Fluor 647. Peptide internalization and PS exposure were followed from the first image acquired (t = 0) up to 20 min by confocal microscopy. The scale bar corresponds to 20 μm. Brightness and contrast were adjusted individually to optimize visualization.

When investigating the nature of the membrane accumulation of the TP10 analog Gly2 → *L*-CF_3-Bpg, we found that it could be reduced either by a heparinase pre-treatment or by co-incubating the peptides with HS chains. In addition, in HS-poor Jurkat cells, no membrane staining was evident for the TP10 analogs at low concentrations, providing further support for the idea that the aggregation of TP10 analogs on the plasma membrane of HeLa cells is an HS-dependent process. Our demonstration that the amphipathic cationic TP10 peptides have the capacity to engage in interactions with HS on the cell surface is consistent with earlier results showing that cationic complexes containing amphipathic peptides, *e.g.* stearylated TP10, could be efficiently decomplexed *in vitro* by heparin [53]. Nevertheless, the observation that a heparinase treatment did not abolish the membrane staining completely indicates that other membrane components, *e.g.* chondroitin sulfate chains or sialic acid residues, may also be involved in the membrane accumulation of TP10 Gly2 → *L*-CF_3-Bpg. Alternatively, as suggested by the capacity of TP10 wt to disturb the lipid bilayer, the peptide may also interact more strongly with the plasma membrane in the absence of HS. Interestingly, peptide uptake in HeLa correlated positively with uptake in Jurkat cells for a set of TP10 analogs. This parallel behavior further confirms the notion that uptake efficiency is independent of the ability to accumulate on the plasma membrane in an HS-dependent manner. This observation is in contrast to earlier observations for *D*- and *L*-R9. Here, uptake in Hela cells was higher for *L*-R9 than for the *D*-counterpart while for Jurkat cells both peptides showed the same uptake efficiency [18]. The findings are, however, reminiscent of those found by Jiao et al., who for a set of peptides did not find a correlation between membrane affinity and uptake efficiency [54]. One should be aware of the fact that our uptake studies were exclusively dependent on measurements of fluorescence, which may be subject to changes in fluorescence intensity at lower pH values and due to collision-quenching. However, extensive investigations into the possibility and extent of measurement artifacts that we performed in a previous study indicated that these effects are rather small, and that valid conclusions can be drawn from flow cytometry studies [18], provided that the differences are sufficiently clear, as is the case here. Also, fluorescein shows little direct membrane interactions [55] compared for example to rhodamine fluorophores (general experiences from our lab), and is therefore exquisitely suited for purposes such as the real-time imaging and subcellular distribution experiments performed in the context of this study. In itself, the membrane accumulation of TP10 analogs in an HS-dependent manner was surprising to us, since these peptides do not contain any arginines. No affinity could be determined for TP10 wt or TP10 Gly2 → *L*-CF_3-Bpg using isothermal titration calorimetry and it is well known that lysine-only peptides have rather low HS affinities. The reason for the lower affinity is the 2.5-fold lower enthalpic contribution of the binding of lysines to heparin compared to the binding of arginines [56]. The effect of exchanging lysine- and arginine-residues has been directly tested for a number of HS ligands, all showing much lower affinities for lysine-containing HS ligands [56–58].

The above observations, together with the lack of an effect of heparinase treatment on internalization, indicate that TP10 and its analogs do not engage with HS in a manner that leads to subsequent internalization, as has been described for arginine-rich CPPs as well as for a variety of unrelated proteoglycan ligands [25,28–31]. Combined with our earlier findings on *D- versus L*-CPP, the findings thus lead us to propose that cell-penetrating peptides may interact with heparan sulfates in at least three functionally distinct manners that lead to different outcomes with

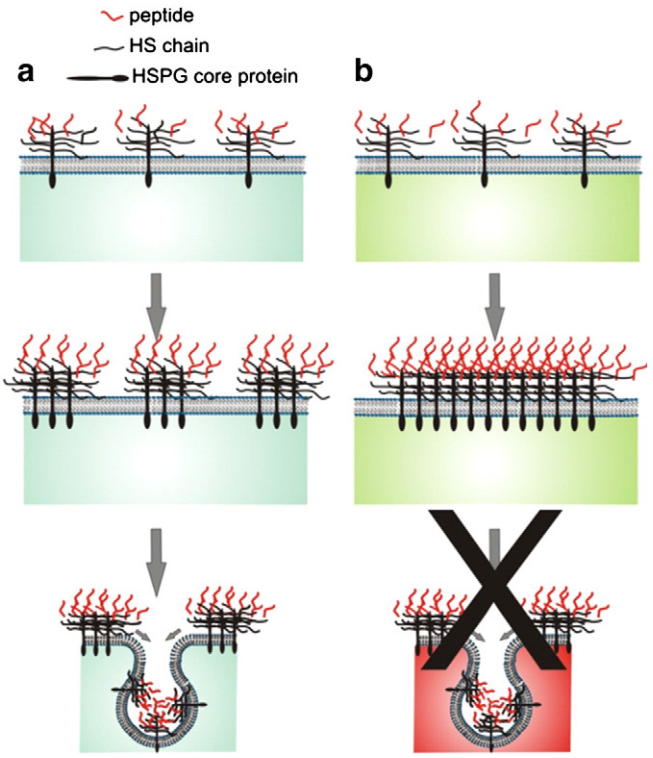


Fig. 6. Scheme for the proposed engagement of heparan sulfate chains in two distinct ways. a) Binding of peptides or other HS ligands leads to cluster formation, which then stimulates uptake through the activation of intracellular signaling cascades. b) Binding of peptides to HS leads to large peptide–HS clusters that are unproductive with regard to peptide uptake.

respect to internalization. For arginine-rich peptides with a negative binding enthalpy, binding leads to uptake in a stereochemistry-dependent manner, which means that binding either induces uptake (L-analogs) or peptides remain sequestered by the glycocalyx (D-analogs). Third, for amphipathic CPP large clusters are formed on the plasma membrane that are unproductive for cell uptake (Fig. 6).

Currently, the size of HS clusters has not been directly assessed on the plasma membrane. Padari et al. have recently directly assessed peptide-dependent differences of cluster size and shape on the plasma membrane for variants of the $S4_{13}$-PV peptide. Specifically, they found that reversing or scrambling the nuclear localization signal (NLS) in this peptide led to larger and more irregular structures on the plasma membrane, though the precise relationship of these findings to uptake efficiency was not addressed [34].

Next to the assessment of cluster size, it would be highly interesting to directly assess the effects on the activation of downstream signaling cascades, *e.g.* Rac1 activation, that lead to peptide internalization. Also, it is not directly apparent how the large HS-containing CPP clusters observed here differ from HS clusters induced by the interaction of cells with cationic polyplexes for which syndecans promote uptake [59]. An interesting possibility that requires further research is that the sheer size of the CPP aggregates prevents their internalization.

Recently, Amand et al. showed for penetratin and two variants containing either only lysine or only arginine residues that peptide uptake did not correlate with the affinity for the plasma membrane. Instead, the internalization efficiency correlated well with the ability to induce heparin clustering [58], even though overall there was little difference in the cell association between GAG-containing and GAG-deficient cells. In view of our results for arginine-rich and amphipathic CPP, these findings may also relate to the characteristics of penetratin. Besides GAGs, other "undefined factors" were also deemed of importance in determining the difference in uptake efficiency. Ziegler et al. showed that the coupling of WR9 to a PEG chain resulted in the loss of the ability to induce GAG clustering. Whereas this modification resulted in only a moderately reduced affinity for HS chains, uptake was much lower, which they attributed to the inability of PEGylated WR9 to cluster HS chains. Interestingly, they found that uptake was much more reduced at 10 μM than at 2 μM, which they interpreted by saying that clustering is mainly required for direct translocation at higher peptide concentrations [22].

Metabolic sugar labeling provided a powerful means to fluorescently tag the glycocalyx and assess the colocalization of peptide aggregates with sugar clusters. In our case, we employed a sugar precursor that labeled sialic acids. While sialic acids are abundant posttranslational protein modifications next to cell surface glycosaminoglycan chains (*e.g.* HS), this strategy nevertheless provides powerful means to monitor the impact of CPP-membrane binding on sugar redistribution. The use of this approach to visualize the membrane proximal sialic acid moieties simultaneously with CPP binding dynamics to membrane distal located GAG chains prevents interference between potential recognition epitopes within the HS and the used CPPs. While in this way also glycan residues of proteins that did not carry HS were labeled, the absence of sialic acid clusters colocalizing with peptide aggregates following HS removal demonstrated that this approach enabled the monitoring of peptide induced glycosaminoglycan redistribution by time-lapse microscopy. Regarding the membrane behavior of TP10 in comparison to arginine-rich peptides, previous studies have indicated that TP10 already causes membrane disturbances and/or effects on cell proliferation at much lower concentrations compared to arginine-rich peptides such as TAT or penetratin in both adherent and suspension cell lines [60,61]. Our study further supports the differences in the membrane behavior of arginine-rich CPP and TP10 through the comparison of R9 and TP10 with respect to their ability to induce PS exposure, a classical marker of membrane disturbance. Whereas at high concentrations R9 only caused local exposure of PS [51,52], TP10 at high concentrations caused a rapid exposure of PS over the whole cell in a matter of minutes. This result clearly indicates that next to differences in HS engagement different interactions also occur at the plasma membrane for R9 and TP10. Interestingly, TP10 Gly2 → *L*-CF_3-Bpg did not lead to any detectable PS exposure in HeLa cells at 25 μM, presumably because the peptide is effectively sequestered by the HS layer. Although not directly assessed, it is very likely that at this concentration TP10 wt is much more toxic due its capacity to directly interact with the plasma membrane.

In conclusion, our findings refute the general notion that GAG clustering always productively stimulates cellular uptake pathways. In contrast, TP10 analogs cluster with HS on the plasma membrane in a manner that is unproductive for uptake.

Acknowledgments

We thank Mattias Hällbrink for helpful discussions and we thank Floris van Delft for helpful discussions concerning metabolic labeling. W.P.R.V. was supported from funds of the Radboud University Nijmegen Medical Centre, R.W. was supported by BMBF Biotransporter (13N11454), S.S. by funds from the Roche Postdoc Programme. A.S.U. acknowledges the DFG-Center for Functional Nanostructures (TP E1.2).

Appendix A. Supplementary data

Supplementary data to this article can be found online at http://dx.doi.org/10.1016/j.jconrel.2013.05.001.

References

[1] F. Duchardt, M. Fotin-Mleczek, H. Schwarz, R. Fischer, R. Brock, A comprehensive model for the endocytic uptake of cationic cell-penetrating peptides, Traffic 8 (2007) 848–866.
[2] F. Madani, S. Lindberg, U. Langel, S. Futaki, A. Graslund, Mechanisms of cellular uptake of cell-penetrating peptides, J. Biophys. 2011 (2011) 414729.
[3] W.P. Verdurmen, R. Brock, Biological responses towards cationic peptides and drug carriers, Trends Pharmacol. Sci. 32 (2011) 116–124.

[4] G. Tunnemann, R.M. Martin, S. Haupt, C. Patsch, F. Edenhofer, M.C. Cardoso, Cargo-dependent mode of uptake and bioavailability of TAT-containing proteins and peptides in living cells, FASEB J. 20 (2006) 1775–1784.
[5] J. Mueller, I. Kretzschmar, R. Volkmer, P. Boisguerin, Comparison of cellular uptake using 22 CPPs in 4 different cell lines, Bioconjug. Chem. 19 (2008) 2363–2374.
[6] E. Vives, P. Brodin, B. Lebleu, A truncated HIV-1 Tat protein basic domain rapidly translocates through the plasma membrane and accumulates in the cell nucleus, J. Biol. Chem. 272 (1997) 16010–16017.
[7] P.A. Wender, D.J. Mitchell, K. Pattabiraman, E.T. Pelkey, L. Steinman, J.B. Rothbard, The design, synthesis, and evaluation of molecules that enable or enhance cellular uptake: peptoid molecular transporters, Proc. Natl. Acad. Sci. 97 (2000) 13003–13008.
[8] U. Soomets, M. Lindgren, X. Gallet, M. Hallbrink, A. Elmquist, L. Balaspiri, M. Zorko, M. Pooga, R. Brasseur, U. Langel, Deletion analogues of transportan, Biochim. Biophys. Acta 1467 (2000) 165–176.
[9] M. Pooga, U. Soomets, M. Hallbrink, A. Valkna, K. Saar, K. Rezaei, U. Kahl, J.X. Hao, X.J. Xu, Z. Wiesenfeldhallin, T. Hokfelt, A. Bartfai, U. Langel, Cell penetrating PNA constructs regulate galanin receptor levels and modify pain transmission in vivo, Nat. Biotechnol. 16 (1998) 857–861.
[10] P. Lundin, H. Johansson, P. Guterstam, T. Holm, M. Hansen, U. Langel, S. El Andaloussi, Distinct uptake routes of cell-penetrating peptide conjugates, Bioconjug. Chem. 19 (2008) 2535–2542.
[11] K. Padari, P. Saalik, M. Hansen, K. Koppel, R. Raid, U. Langel, M. Pooga, Cell transduction pathways of transportans, Bioconjug. Chem. 16 (2005) 1399–1410.
[12] E. Goncalves, E. Kitas, J. Seelig, Structural and thermodynamic aspects of the interaction between heparan sulfate and analogues of melittin, Biochemistry 45 (2006) 3086–3094.
[13] A. Ziegler, J. Seelig, Binding and clustering of glycosaminoglycans: a common property of mono- and multivalent cell-penetrating compounds, Biophys. J. 94 (2008) 2142–2149.
[14] L.E. Yandek, A. Pokorny, P.F. Almeida, Small changes in the primary structure of transportan 10 alter the thermodynamics and kinetics of its interaction with phospholipid vesicles, Biochemistry 47 (2008) 3051–3060.
[15] T. Letoha, A. Keller-Pinter, E. Kusz, C. Kolozsi, Z. Bozso, G. Toth, C. Vizler, Z. Olah, L. Szilak, Cell-penetrating peptide exploited syndecans, Biochim. Biophys. Acta 1798 (2010) 2258–2265.
[16] S.M. Fuchs, R.T. Raines, Pathway for polyarginine entry into mammalian cells, Biochemistry 43 (2004) 2438–2444.
[17] F. Duchardt, I.R. Ruttekolk, W.P. Verdurmen, H. Lortat-Jacob, J. Burck, H. Hufnagel, R. Fischer, M. van den Heuvel, D.W. Lowik, G.W. Vuister, A. Ulrich, M. de Waard, R. Brock, A cell-penetrating peptide derived from human lactoferrin with conformation-dependent uptake efficiency, J. Biol. Chem. 284 (2009) 36099–36108.
[18] W.P. Verdurmen, P.H. Bovee-Geurts, P. Wadhwani, A.S. Ulrich, M. Hallbrink, T.H. van Kuppevelt, R. Brock, Preferential uptake of L- versus D-amino acid cell-penetrating peptides in a cell type-dependent manner, Chem. Biol. 18 (2011) 1000–1010.
[19] J.P. Richard, K. Melikov, H. Brooks, P. Prevot, B. Lebleu, L.V. Chernomordik, Cellular uptake of unconjugated TAT peptide involves clathrin-dependent endocytosis and heparan sulfate receptors, J. Biol. Chem. 280 (2005) 15300–15306.
[20] I. Nakase, A. Tadokoro, N. Kawabata, T. Takeuchi, H. Katoh, K. Hiramoto, M. Negishi, M. Nomizu, Y. Sugiura, S. Futaki, Interaction of arginine-rich peptides with membrane-associated proteoglycans is crucial for induction of actin organization and macropinocytosis, Biochemistry 46 (2007) 492–501.
[21] G.M. Poon, J. Gariepy, Cell-surface proteoglycans as molecular portals for cationic peptide and polymer entry into cells, Biochem. Soc. Trans. 35 (2007) 788–793.
[22] A. Ziegler, J. Seelig, Contributions of glycosaminoglycan binding and clustering to the biological uptake of the nonamphipathic cell-penetrating peptide WR9, Biochemistry 50 (2011) 4650–4664.
[23] M. Belting, Heparan sulfate proteoglycan as a plasma membrane carrier, Trends Biochem. Sci. 28 (2003) 145–151.
[24] J.R. Couchman, Transmembrane signaling proteoglycans, Annu. Rev. Cell Dev. Biol. 26 (2010) 89–114.
[25] J.R. Couchman, Syndecans: proteoglycan regulators of cell-surface microdomains? Nat. Rev. Mol. Cell Biol. 4 (2003) 926–937.
[26] I. Kopatz, J.S. Remy, J.P. Behr, A model for non-viral gene delivery: through syndecan adhesion molecules and powered by actin, J. Gene Med. 6 (2004) 769–776.
[27] K.A. Mislick, J.D. Baldeschwieler, Evidence for the role of proteoglycans in cation-mediated gene transfer, Proc. Natl. Acad. Sci. U. S. A. 93 (1996) 12349–12354.
[28] Z.U. Rehman, K.A. Sjollema, J. Kuipers, D. Hoekstra, I.S. Zuhorn, Nonviral gene delivery vectors use syndecan-dependent transport mechanisms in filopodia to reach the cell surface, ACS Nano 6 (2012) 7521–7532.
[29] S. Bacsa, G. Karasneh, S. Dosa, J. Liu, T. Valyi-Nagy, D. Shukla, Syndecan-1 and syndecan-2 play key roles in herpes simplex virus type-1 infection, J. Gen. Virol. 92 (2011) 733–743.
[30] T. Giroglou, L. Florin, F. Schafer, R.E. Streeck, M. Sapp, Human papillomavirus infection requires cell surface heparan sulfate, J. Virol. 75 (2001) 1565–1570.
[31] F.D. Menozzi, V.M. Reddy, D. Cayet, D. Raze, A.S. Debrie, M.P. Dehouck, R. Cecchelli, C. Locht, Mycobacterium tuberculosis heparin-binding haemagglutinin adhesin (HBHA) triggers receptor-mediated transcytosis without altering the integrity of tight junctions, Microbes Infect. 8 (2006) 1–9.
[32] A.V. Dix, L. Fischer, S. Sarrazin, C.P. Redgate, J.D. Esko, Y. Tor, Cooperative, heparan sulfate-dependent cellular uptake of dimeric guanidinoglycosides, ChemBioChem 11 (2010) 2302–2310.
[33] L. Elson-Schwab, O.B. Garner, M. Schuksz, B.E. Crawford, J.D. Esko, Y. Tor, Guanidinylated neomycin delivers large, bioactive cargo into cells through a heparan sulfate-dependent pathway, J. Biol. Chem. 282 (2007) 13585–13591.
[34] K. Padari, K. Koppel, A. Lorents, M. Hallbrink, M. Mano, M.C. Pedroso de Lima, M. Pooga, S4(13)-PV cell-penetrating peptide forms nanoparticle-like structures to gain entry into cells, Bioconjug. Chem. 21 (2010) 774–783.
[35] S. Gerbal-Chaloin, C. Gondeau, G. Aldrian-Herrada, F. Heitz, C. Gauthier-Rouviere, G. Divita, First step of the cell-penetrating peptide mechanism involves Rac1 GTPase-dependent actin-network remodelling, Biol. Cell 99 (2007) 223–238.
[36] J. Imamura, Y. Suzuki, K. Gonda, C.N. Roy, H. Gatanaga, N. Ohuchi, H. Higuchi, Single particle tracking confirms that multivalent Tat protein transduction domain-induced heparan sulfate proteoglycan cross-linkage activates Rac1 for internalization, J. Biol. Chem. 286 (2011) 10581–10592.
[37] J.A. Prescher, C.R. Bertozzi, Chemistry in living systems, Nat. Chem. Biol. 1 (2005) 13–21.
[38] E. Saxon, C.R. Bertozzi, Cell surface engineering by a modified Staudinger reaction, Science 287 (2000) 2007–2010.
[39] J. Dommerholt, S. Schmidt, R. Temming, L.J. Hendriks, F.P. Rutjes, J.C. van Hest, D.J. Lefeber, P. Friedl, F.L. van Delft, Readily accessible bicyclononynes for bioorthogonal labeling and three-dimensional imaging of living cells, Angew. Chem. Int. Ed. Engl. 49 (2010) 9422–9425.
[40] J. Dommerholt, S. Schmidt, R. Temming, L.J.A. Hendriks, F.P.J.T. Rutjes, J.C.M. van Hest, D.J. Lefeber, P. Friedl, F.L. van Delft, Readily accessible bicyclononynes for bioorthogonal labeling and three-dimensional imaging of living cells, Angew. Chem. Int. Ed. 49 (2010) 9422–9425.
[41] C. Foerg, K.M. Weller, H. Rechsteiner, H.M. Nielsen, J. Fernandez-Carneado, R. Brunisholz, E. Giralt, H.P. Merkle, Metabolic cleavage and translocation efficiency of selected cell penetrating peptides: a comparative study with epithelial cell cultures, AAPS J. 10 (2008) 349–359.
[42] C.P. Wan, C.S. Park, B.H. Lau, A rapid and simple microfluorometric phagocytosis assay, J. Immunol. Methods 162 (1993) 1–7.
[43] Z. Ma, L.Y. Lim, Uptake of chitosan and associated insulin in Caco-2 cell monolayers: a comparison between chitosan molecules and chitosan nanoparticles, Pharm. Res. 20 (2003) 1812–1819.
[44] R. Fischer, H. Hufnagel, R. Brock, A doubly labeled penetratin analogue as a ratiometric sensor for intracellular proteolytic stability, Bioconjug. Chem. 21 (2010) 64–73.
[45] A.H. van Asbeck, A. Beyerle, H. McNeill, P.H. Bovee-Geurts, S. Lindberg, W.P. Verdurmen, M. Hallbrink, U. Langel, O. Heidenreich, R. Brock, Molecular parameters of siRNA-cell penetrating peptide nanocomplexes for efficient cellular delivery, ACS Nano (2013), http://dx.doi.org/10.1021/nn305754c (in press).
[46] E. Barany-Wallje, A. Andersson, A. Graslund, L. Maler, NMR solution structure and position of transportan in neutral phospholipid bicelles, FEBS Lett. 567 (2004) 265–269.
[47] M. Lindberg, J. Jarvet, U. Langel, A. Graslund, Secondary structure and position of the cell-penetrating peptide transportan in SDS micelles as determined by NMR, Biochemistry 40 (2001) 3141–3149.
[48] K.J. Yarema, L.K. Mahal, R.E. Bruehl, E.C. Rodriguez, C.R. Bertozzi, Metabolic delivery of ketone groups to sialic acid residues. Application To cell surface glycoform engineering, J. Biol. Chem. 273 (1998) 31168–31179.
[49] E. Eiriksdottir, K. Konate, U. Langel, G. Divita, S. Deshayes, Secondary structure of cell-penetrating peptides controls membrane interaction and insertion, Biochim. Biophys. Acta 1798 (2010) 1119–1128.
[50] O. Maniti, I. Alves, G. Trugnan, J. Ayala-Sanmartin, Distinct behaviour of the homeodomain derived cell penetrating peptide penetratin in interaction with different phospholipids, PLoS One 5 (2010) e15819.
[51] W.P. Verdurmen, M. Thanos, I.R. Ruttekolk, E. Gulbins, R. Brock, Cationic cell-penetrating peptides induce ceramide formation via acid sphingomyelinase: implications for uptake, J. Control. Release 147 (2010) 171–179.
[52] H. Hirose, T. Takeuchi, H. Osakada, S. Pujals, S. Katayama, I. Nakase, S. Kobayashi, T. Haraguchi, S. Futaki, Transient focal membrane deformation induced by arginine-rich peptides leads to their direct penetration into cells, Mol. Ther. 20 (2012) 984–993.
[53] T. Lehto, O.E. Simonson, I. Mager, K. Ezzat, H. Sork, D.M. Copolovici, J.R. Viola, E.M. Zaghloul, P. Lundin, P.M. Moreno, M. Mae, N. Oskolkov, J. Suhorutsenko, C.I. Smith, S.E. Andaloussi, A peptide-based vector for efficient gene transfer in vitro and in vivo, Mol. Ther. 19 (2011) 1457–1467.
[54] C.Y. Jiao, D. Delaroche, F. Burlina, I.D. Alves, G. Chassaing, S. Sagan, Translocation and endocytosis for cell-penetrating peptide internalization, J. Biol. Chem. 284 (2009) 33957–33965.
[55] I.R. Ruttekolk, J.J. Witsenburg, H. Glauner, P.H. Bovee-Geurts, E.S. Ferro, W.P. Verdurmen, R. Brock, The intracellular pharmacokinetics of terminally capped peptides, Mol. Pharm. 9 (2012) 1077–1086.
[56] J.R. Fromm, R.E. Hileman, E.E. Caldwell, J.M. Weiler, R.J. Linhardt, Differences in the interaction of heparin with arginine and lysine and the importance of these basic amino acids in the binding of heparin to acidic fibroblast growth factor, Arch. Biochem. Biophys. 323 (1995) 279–287.
[57] A. Rullo, M. Nitz, Importance of the spatial display of charged residues in heparin-peptide interactions, Biopolymers 93 (2010) 290–298.
[58] H.L. Amand, H.A. Rydberg, L.H. Fornander, P. Lincoln, B. Norden, E.K. Esbjorner, Cell surface binding and uptake of arginine- and lysine-rich penetratin peptides in absence and presence of proteoglycans, Biochim. Biophys. Acta 1818 (2012) 2669–2678.
[59] S. Paris, A. Burlacu, Y. Durocher, Opposing roles of syndecan-1 and syndecan-2 in polyethyleneimine-mediated gene delivery, J. Biol. Chem. 283 (2008) 7697–7704.
[60] K. Saar, M. Lindgren, M. Hansen, E. Eiriksdottir, Y. Jiang, K. Rosenthal-Aizman, M. Sassian, U. Langel, Cell-penetrating peptides: a comparative membrane toxicity study, Anal. Biochem. 345 (2005) 55–65.
[61] S. El-Andaloussi, P. Jarver, H.J. Johansson, U. Langel, Cargo-dependent cytotoxicity and delivery efficacy of cell-penetrating peptides: a comparative study, Biochem. J. 407 (2007) 285–292.

Supplementary Materials to

Cell surface clustering of heparan sulfate proteoglycans by amphipathic cell-penetrating peptides does not contribute to uptake

Wouter P. R. Verdurmen[a], Rike Wallbrecher[a], Samuel Schmidt[a], Jos Eilander[a], Petra Bovee-Geurts[a], Susanne Fanghänel[b], Jochen Bürck[c], Parvesh Wadhwani[c], Anne S. Ulrich[b,c], Roland Brock[a]

[a]Department of Biochemistry, Nijmegen Centre for Molecular Life Sciences, Radboud University Nijmegen Medical Centre, Post 286, PO box 9101, 6500 HB Nijmegen, The Netherlands

[b]Karlsruhe Institute of Technology (KIT), Institute for Organic Chemistry and CFN, Fritz-Haber-Weg 6, 76131 Karlsruhe, Germany

[c]KIT, Institute for Biological Interfaces (IBG-2), P.O.B. 3640, 76021 Karlsruhe, Germany

Corresponding author: Prof. Dr. Roland Brock
Department of Biochemistry, Nijmegen Centre for Molecular Life Sciences, Radboud University Nijmegen Medical Centre. Post 286, PO box 9101, 6500 HB Nijmegen, The Netherlands

E-mail: R.Brock@ncmls.ru.nl. Tel: +31 (0) 24 361 42 59. Fax: +31 (0) 24 361 64 13

Supplementary figures

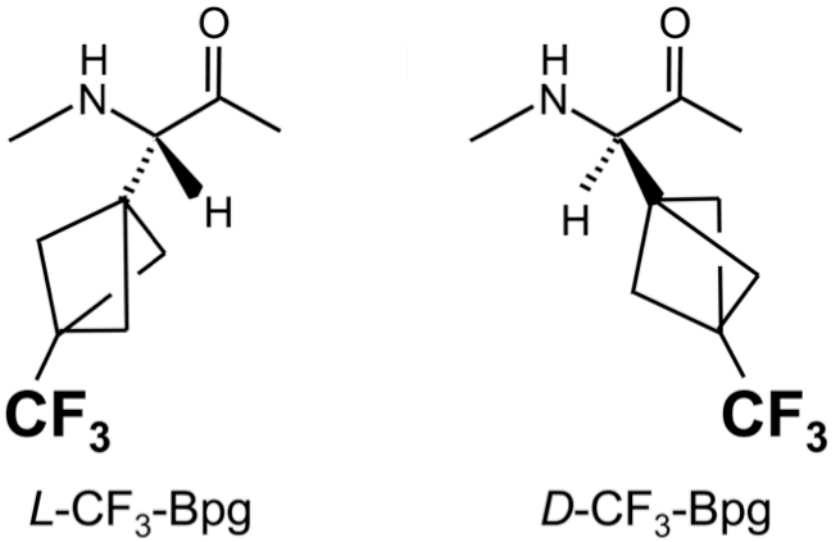


Figure S1. Chemical structure of trifluoromethyl-bicyclopent-[1.1.1]-1-yl-glycine (CF_3-Bpg); (A) *L*-CF_3-Bpg, (B) *D*-CF_3-Bpg.

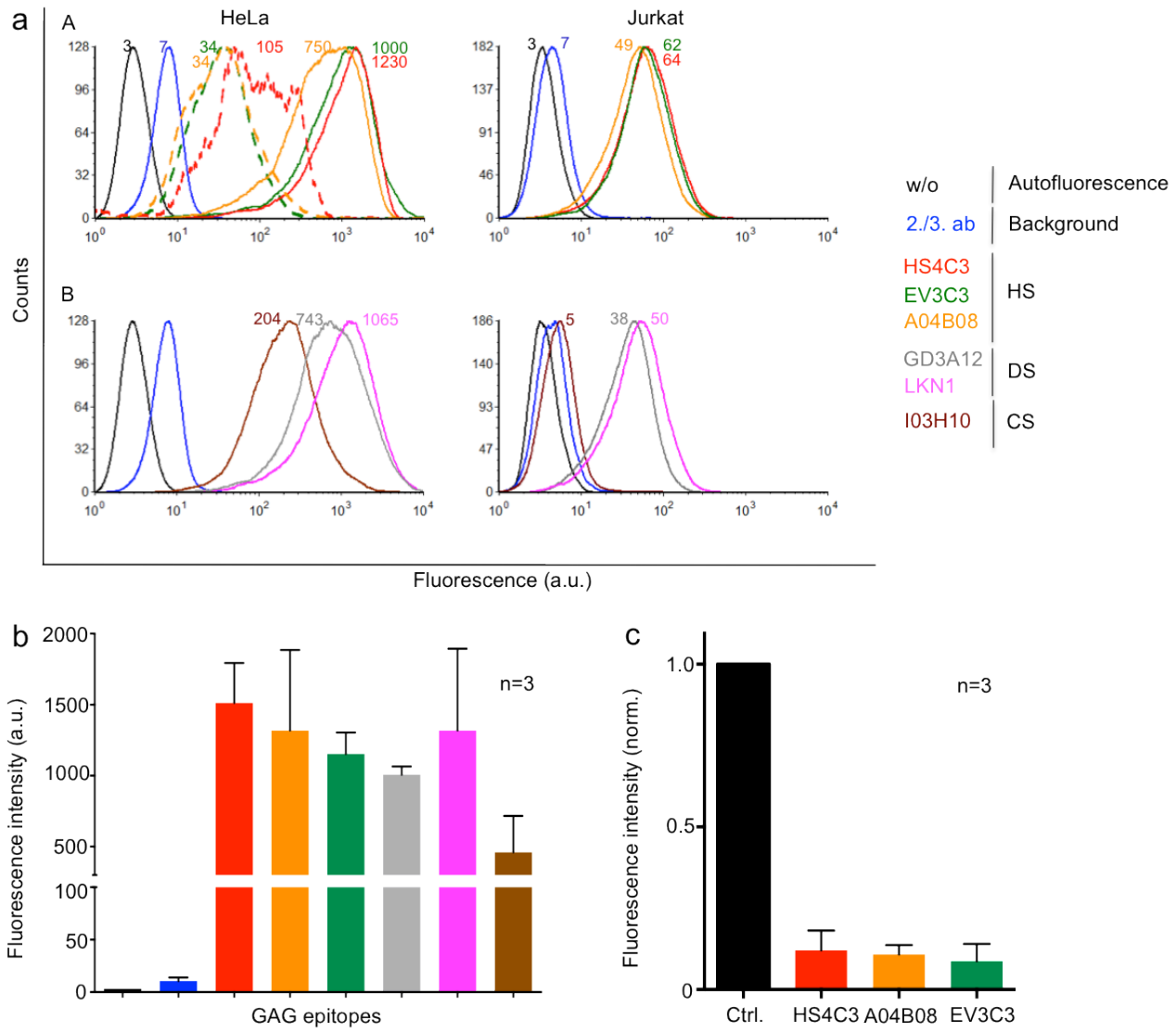


Figure S2. GAG profiling of HeLa and Jurkat cells by flow cytometry. Expression of cell surface GAGs was measured after incubation with single chain antibody fragments directed against epitopes on heparan sulfates (HS)-, dermatan sulfates (DS)- and chondroitin sulfates (CS) chains. Efficient enzymatic degradation of HS chains with cells in suspension, leading to comparable expression levels to Jurkat cells, was performed by treatment of cells with 3 mIU of heparinase III (dashed traces). Fluorescence represents median fluorescence intensities. (a) Flow cytometry histograms of one representative experiment; (b, c) Average intensities and standard deviations (SD) of (b) two and (c) three independent experiments showing (b) expression levels on Hela cells and (c) expression of HS epitopes after enzymatic removal normalized to expression levels of untreated cells. Hela cells were detached with 1 mM EDTA-containing PBS resuspended in RPMI1640 culture medium containing 1% FCS with or without GAG-degrading enzymes. Jurkat cells were washed with RPMI 1640 culture medium containing 1% FCS and then treated in the same way as HeLa cells.. Cells were

washed afterwards three times with 1X HBS and incubated with anti-HS single chain antibodies, recognizing certain epitopes within the HS GAG chains, IdoA2S-GlcNS3S6S (HS4C3V-vsv) [1], IdoA2S-GlcNS6S (A04B08V-vsv) [2] and GlcNS +/- 6S-GlcA/IdoA2S (EV3C3V-vsv) [3], anti-DS single chain antibodies, recognizing the epitopes 4/2,4-di-OS (LKN1V-vsv) [4] and IdoA-Gal-NAc4S (GD3A12V-vsv) [5] and the anti-CS single chain antibody, recognizing the epitope GlcA-GalNAc6S (I03H10V-vsv) [6] for 30 min at 4°C. Cells were again washed three times with 1X HBS and incubated with the 2nd mouse-anti vsv (P5D4) for 30 min at 4°C. After washing cells were finally incubated with a goat-anti-mouse IgG Alexa Fluor 488 conjugated antibody (Invitrogen) for 30 min at 4°C, followed by washing steps and Flow cytometry measurements.

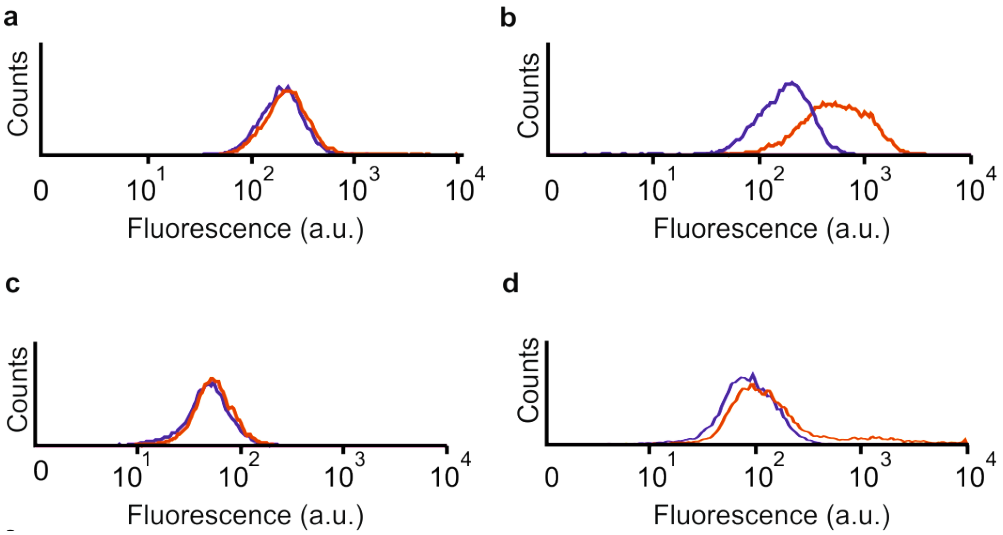


Figure S3. Flow cytometry overlay images (c-d) and quantification (e) of the uptake of TP10 (a,c) and TP10 Gly2→*L*-CF_3-Bpg (b,d) in HeLa (a,b) and Jurkat cells (c,d). Cells were incubated for 1 h at 37°C in 24-well plates with 5 μM of the indicated peptide. After washing the cells by centrifugation and/or trypsinization (only HeLa cells), cells were resuspended in medium in the presence (blue curves) or absence (red curves) of trypan blue.

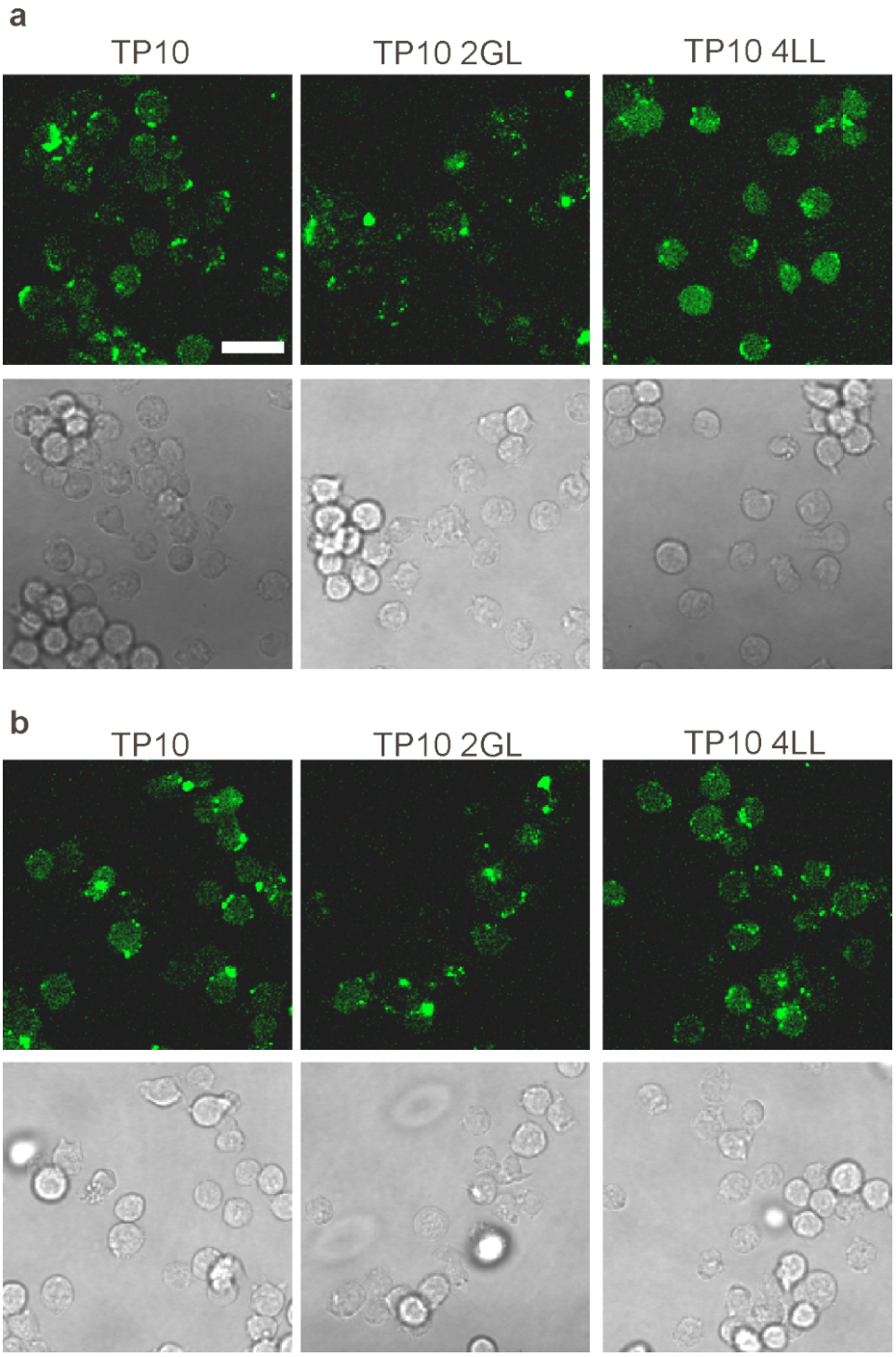
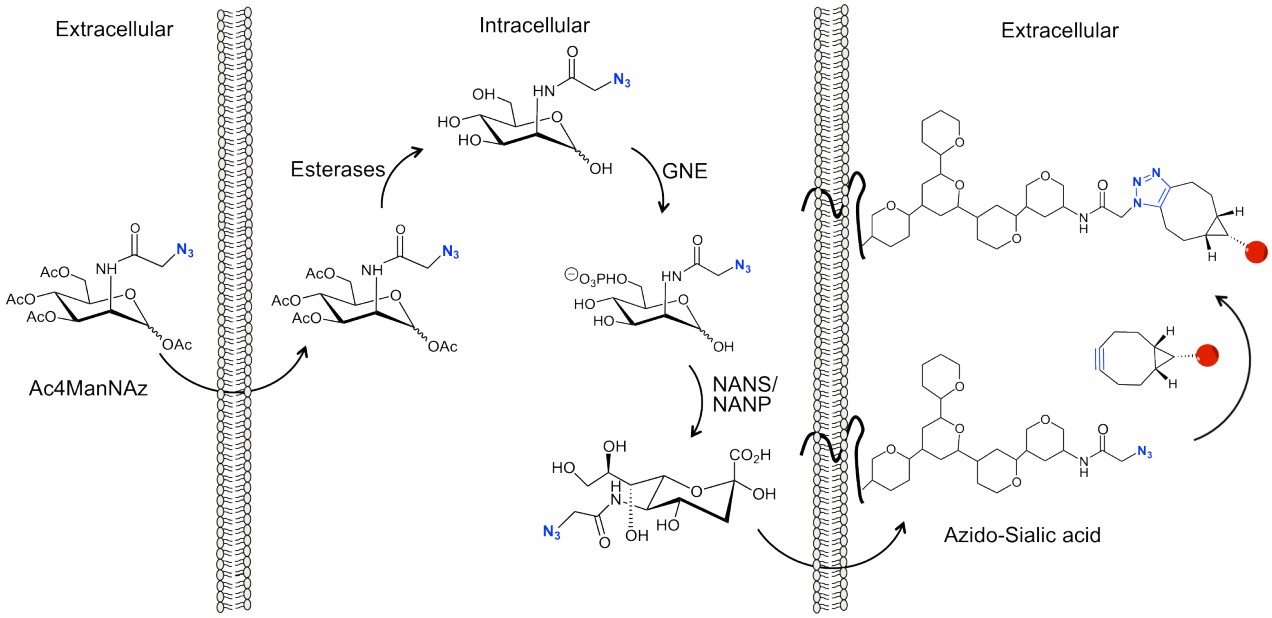


Figure S4. Effect of the cysteine protease inhibitor E64d on the intracellular distribution of TP10 (analogs). Jurkat cells were (a) left untreated or (b) preincubated with 100 µM E64d in serum-free medium for 30 min at 37°C. This preincubation was followed by an incubation with 2.5 µM of the indicated peptides in RPMI + 10% FCS for 1 h at 37°C without (a) or with (b) E64d. The scale bar corresponds to 20 µm.



Figures S5. Bioorthogonal labeling procedure of cells. Incorporation of ManNAz, an azido derivate of ManNAc, into cells allows detection of cell surface sialic acids. Peracetylated N-azidoacethylmannosamine (Ac4ManNAz) can be taken up and comparably metabolized and used as other hexosamines. Exogenously added Ac4ManNAz diffuses into the cell and is deacetylated by intracellular esterases, and then enters into the salvage pathway, including phosphorylation of ManNAz to ManNAc-6-Phosphate by UDP-GlcNAc 2-epimerase/ManNAc-6- kinase (GNE) as the key enzyme in sialic acid biosynthesis, generation of phosphorylated Neu5Ac (Neu5Ac-9-phosphate) by N-acetylneuraminic acid synthase (Neu5Ac-9-P synthetase/NANS) and dephosphorylation of Neu5Ac by N-acetylneuraminic-acid Phosphatase (Neu5Ac-9-P Phosphatase/NANP) before entering the nucleus. Further modifications in the nucleus and the golgi apparatus take place, that involves CMP-Neu5Ac-Synthetase (CMAS) and SLC35A1 (solute carrier family 35/CMP-sialic acid transporter) and sialyltransferases (ST) before the azido-sialic acids appear as part of glycan moities of glycoproteins at the cell surface. [7-9]. The detection of cell surface azido-sialic acids can be performed by using e.g. biotin-conjugated Bicyclo [6.1.0] nonyne (BCN) in a metal-free strain promoted alkyne-azide cycloaddition (SPAAC) reaction, giving stable 1,2,3-triazoles. Finally, a fluorophore-conjugated streptavidin can be used to visualize bioorthogonal labeled sialic acids using e.g. confocal microscopy [10].

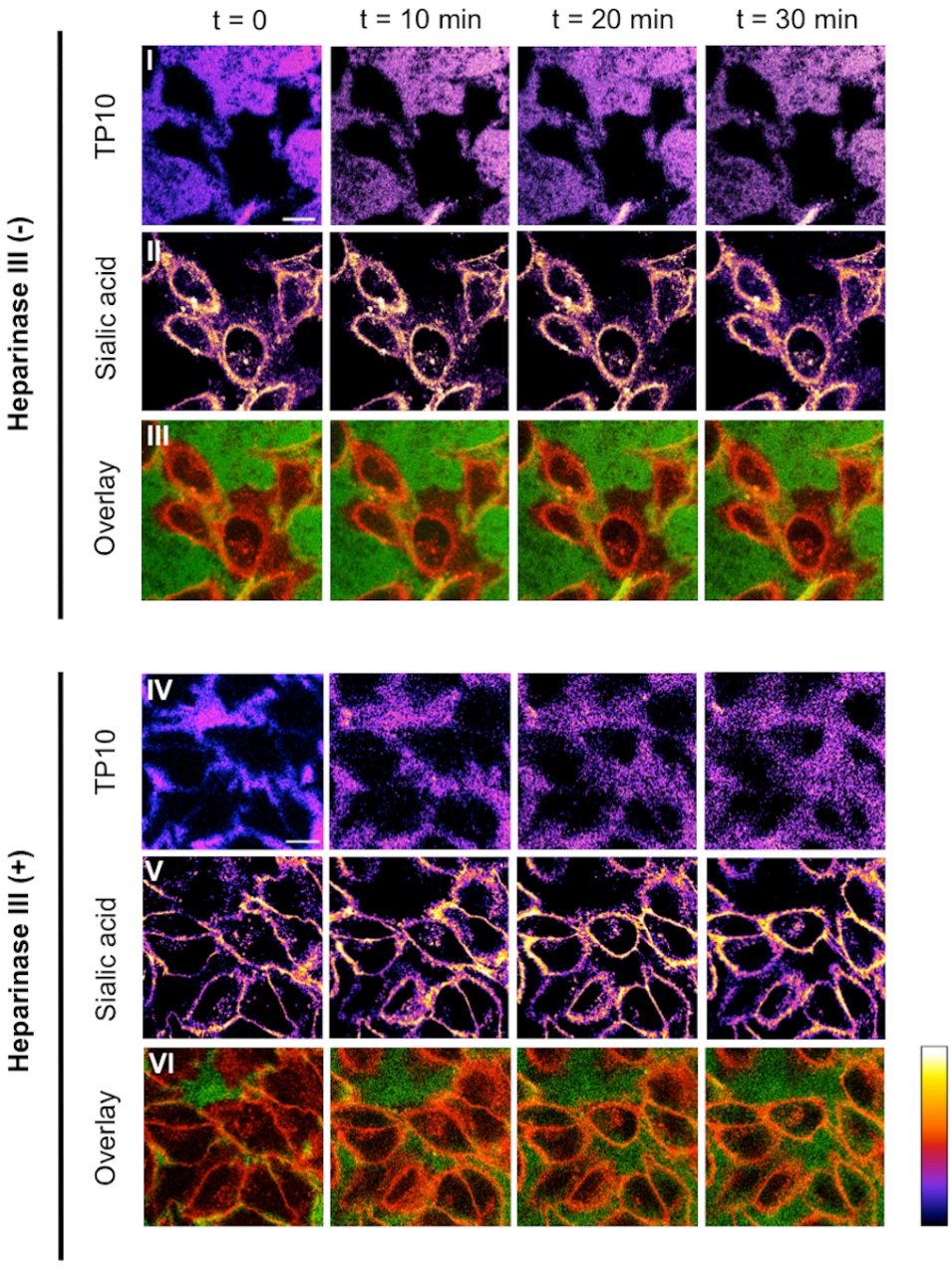


Figure S6. Time-lapse of the uptake of TP10 WT in HeLa cells. HeLa cells were incubated with 5 mM of the peptide with or without a pre-treatment with heparinase III. (a, d) False color representations of the peptide, (b, e) the sialic acid stain and (c, f) overlays of peptide and sialic acid with peptide depicted in green and sialic acid in red. The false color look-up table ranges from black (low) to white (high). The scale bar corresponds to 20 μm.

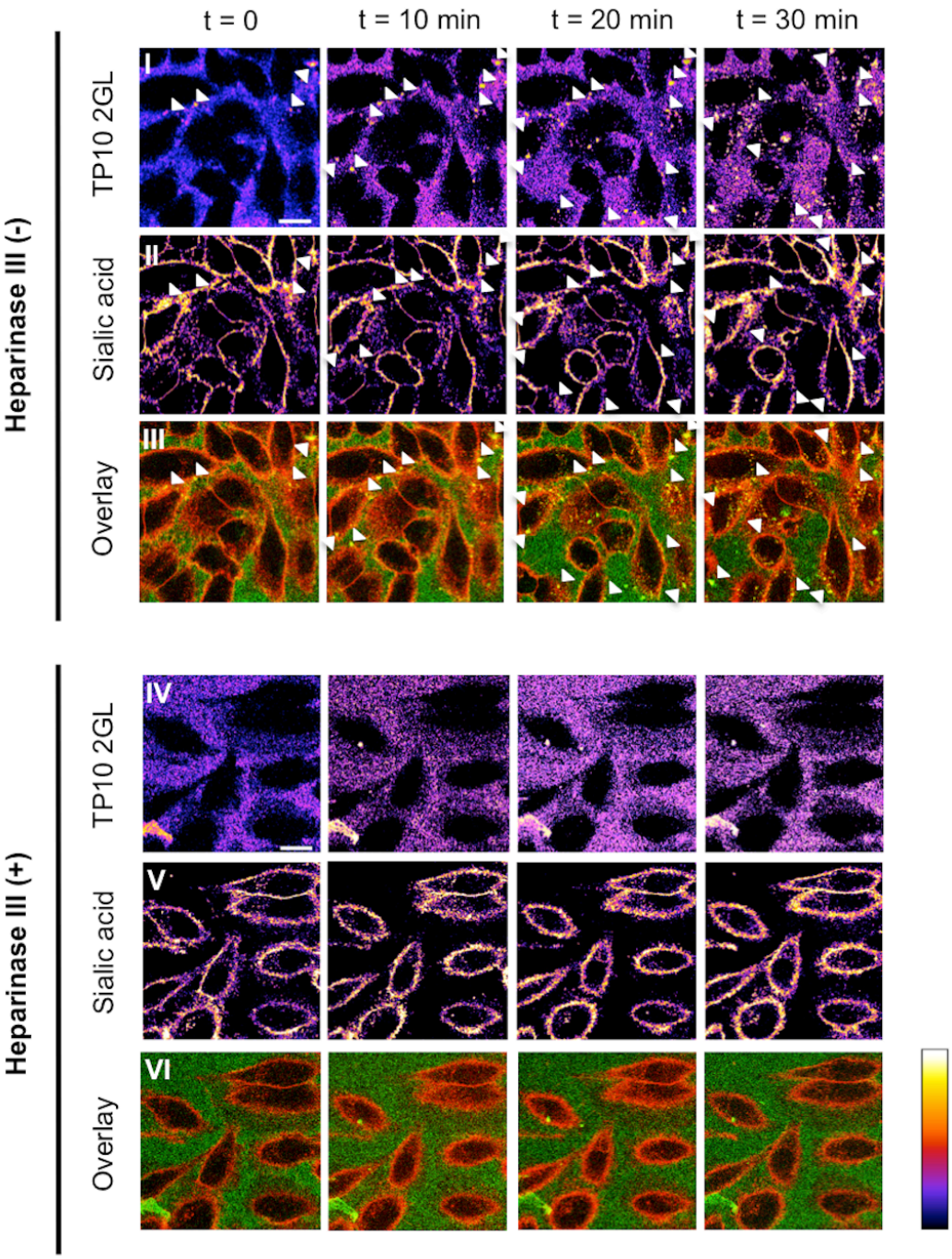


Figure S7. Time-lapse of the uptake of TP10 Gly2→*L/D*-CF_3-Bpg in HeLa cells. HeLa cells were incubated with 5 μM of the peptide with or without a pre-treatment with heparinase III. (a, d) False color representations of the peptide, (b, e) the sialic acid stain and (c, f) overlays of peptide and sialic acid with peptide depicted in green and sialic acid in red. Sites of coclustering of peptide and the glycocalyx are depicted by arrows. The false color look-up table ranges from black (low) to white (high). The scale bar corresponds to 20 μm.

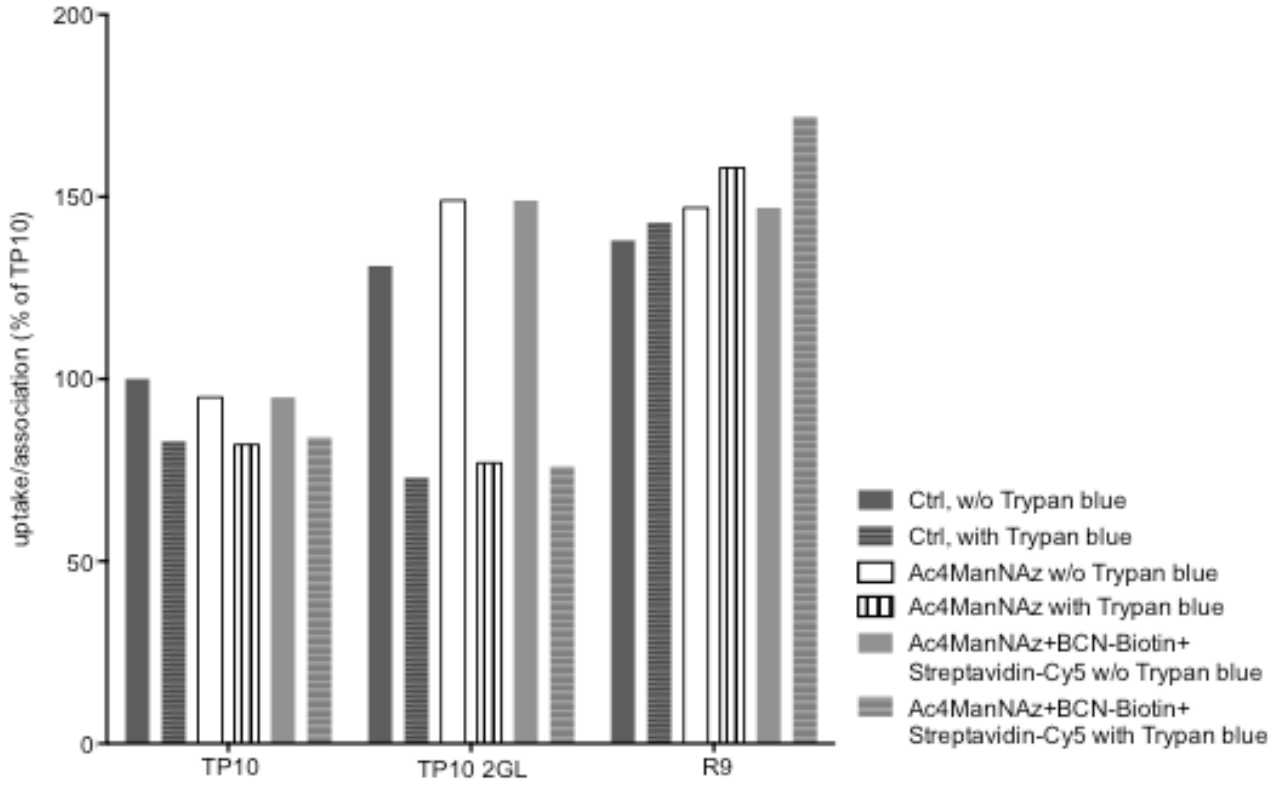


Figure S8: Impact of the bioorthogonal labeling on cell surface binding and uptake. HeLa cells were cultured over night in the presence or absence of Ac4ManNAz (50 µM), followed by labeling of incorporated azido sialic acid moieties with a bicyclo[6.1.0]nonyne (BCN)-biotin conjugate and secondary labeling with streptavidin-Cy5. For analysing the impact of incorporated azido sialic acid alone on binding to the cell surface and uptake oft he administered CPP, cells were incubated with Ac4ManNAz (50 µM), but labeling with BCN-biotin conjugate and secondary labeling with streptavidin-Cy5 were omitted. Subsequentely, TP10, TP10 2GL or R9 were administered in a final concentration of 5µM, incubated for 1 hour at 37°C, 5% CO_2 and measured in FACS.

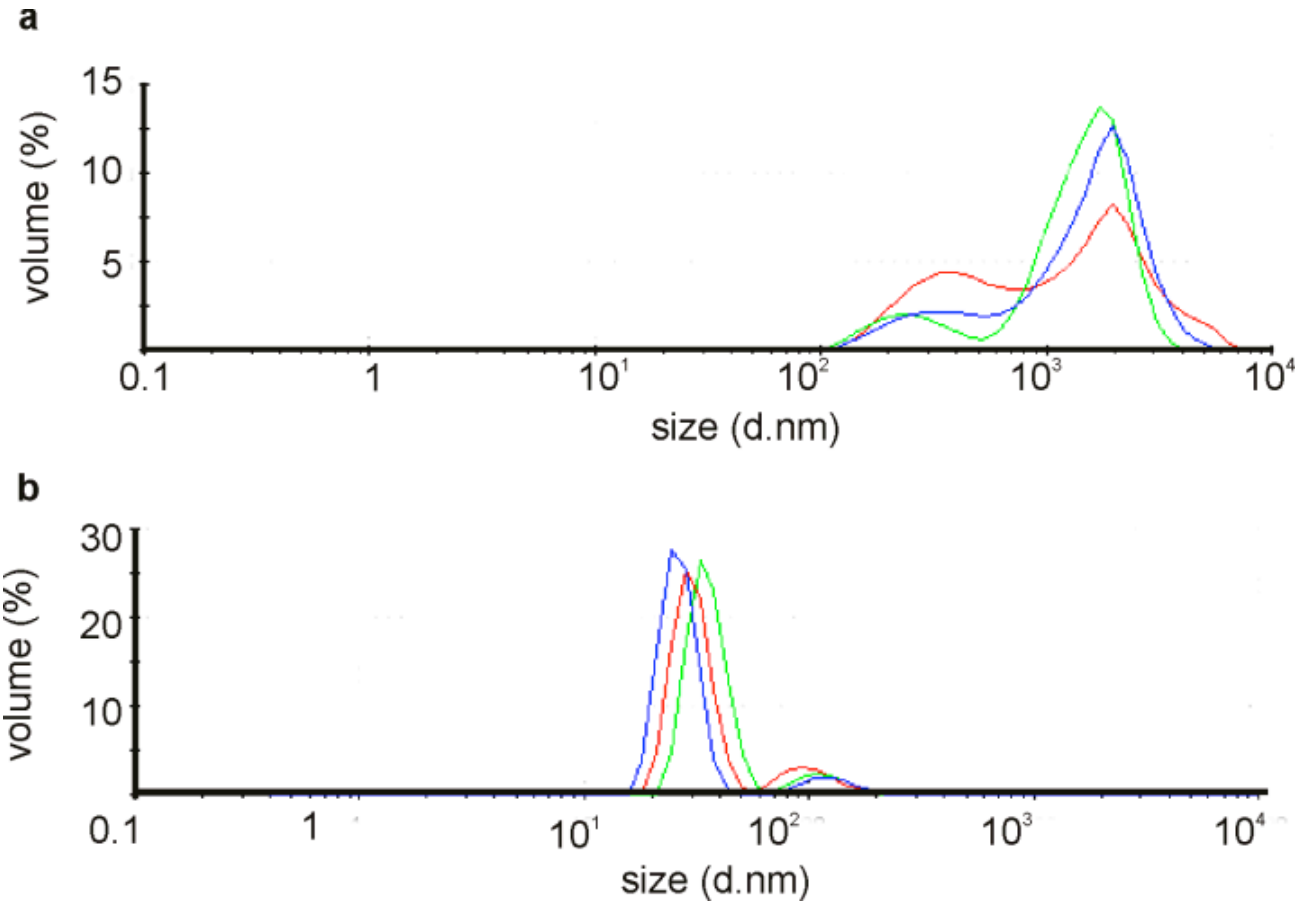


Figure S9. Size distribution of clusters formed by co-incubating R9 and TP10 Gly2→L-CF_3-Bpg with HS chains. The size distribution by volume of clusters that originate from co-incubation of 5 μM TP10 Gly2→L-CF_3-Bpg (a) and 5 μM R9 (b) with 10 μM HS chains. Three successive measurements are shown for each peptide. Each measurement consisted of six runs of 10 s, performed at 37°C. Both peptides were fluorescein-labeled. DLS experiments were performed with a Zetasizer Nano S (Malvern Instruments Ltd, Malvern, UK). Equilibration time before measurements was 20 s. Initially, 100 μl of a 5 μM peptide solution was added into ZEN0040 disposable microcuvettes. Then, HS was added to the cuvettes to a concentration of 10 μM. Samples were then briefly mixed by pipetting up and down and measured directly afterwards.

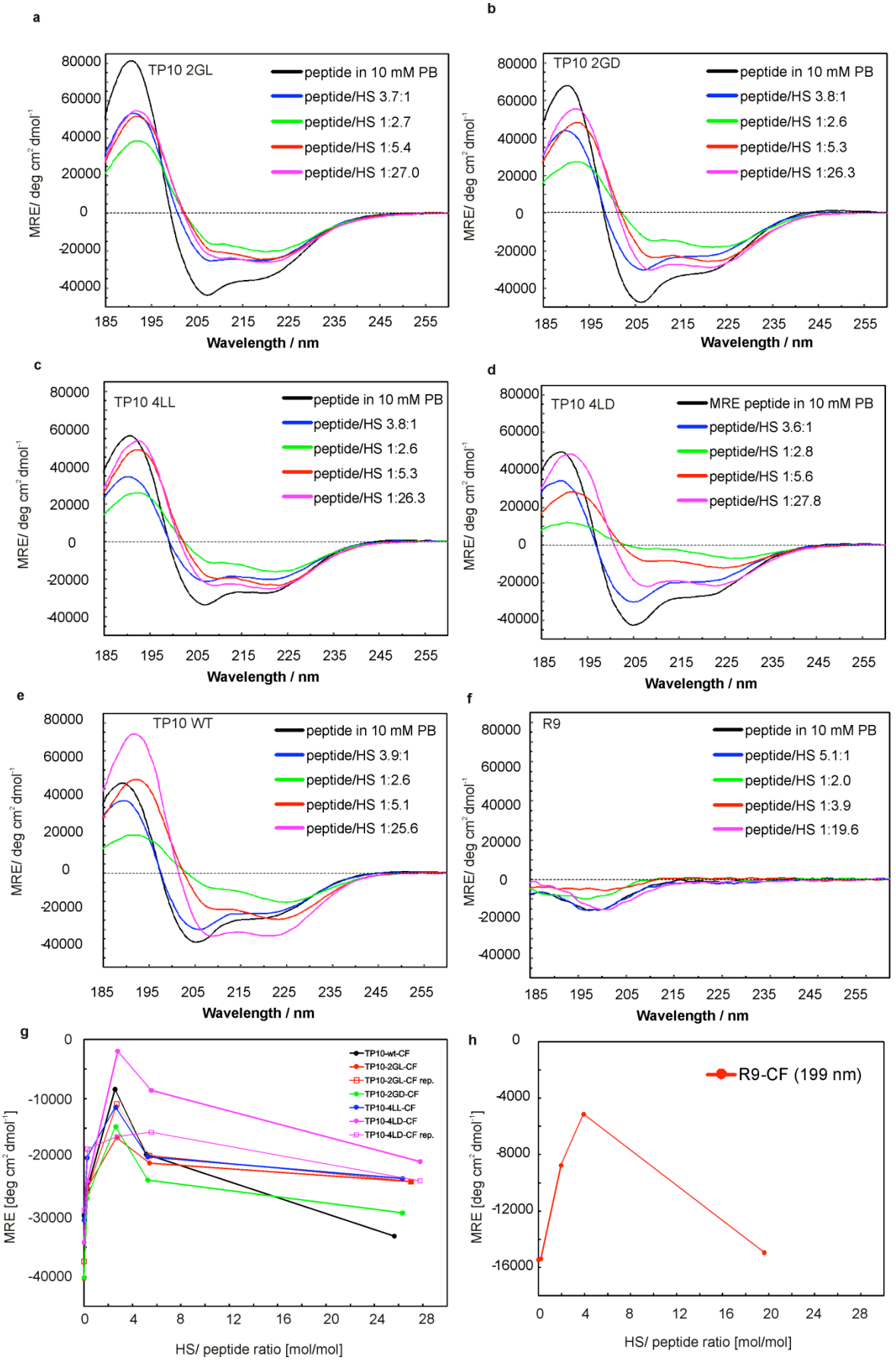

a
TP10 2GL
peptide in 10 mM PB
peptide/HS 3.7:1
peptide/HS 1:2.7
peptide/HS 1:5.4
peptide/HS 1:27.0
MRE/ deg cm2 dmol-1
Wavelength / nm
b
TP10 2GD
peptide in 10 mM PB
peptide/HS 3.8:1
peptide/HS 1:2.6
peptide/HS 1:5.3
peptide/HS 1:26.3
c
TP10 4LL
peptide in 10 mM PB
peptide/HS 3.8:1
peptide/HS 1:2.6
peptide/HS 1:5.3
peptide/HS 1:26.3
d
TP10 4LD
MRE peptide in 10 mM PB
peptide/HS 3.6:1
peptide/HS 1:2.8
peptide/HS 1:5.6
peptide/HS 1:27.8
e
TP10 WT
peptide in 10 mM PB
peptide/HS 3.9:1
peptide/HS 1:2.6
peptide/HS 1:5.1
peptide/HS 1:25.6
f
R9
peptide in 10 mM PB
peptide/HS 5.1:1
peptide/HS 1:2.0
peptide/HS 1:3.9
peptide/HS 1:19.6
g
TP10-wt-CF
TP10-2GL-CF
TP10-2GL-CF rep.
TP10-2GD-CF
TP10-4LL-CF
TP10-4LD-CF
TP10-4LD-CF rep.
MRE [deg cm2 dmol-1]
HS/ peptide ratio [mol/mol]
h
R9-CF (199 nm)
MRE [deg cm2 dmol-1]
HS/ peptide ratio [mol/mol]

Figure S10. Circular dichroism of R9 and TP10 and analogs in pure phosphate buffer (PB) and in the presence of HS chains. a-f) CD spectra in the presence of increasing amounts of HS. The peptides used are indicated in the graphs. g) The MRE at 210 nm vs HS/peptide ratio for TP10 wt and TP10 analogs. h) The MRE at 199 nm vs HS/peptide ratio for R9. All peptides were fluorescently labeled. MRE = mean residue ellipticity; CD = circular dichroism.TP10 2GL/D = TP10 Gly2→*L/D*-CF_3-Bpg; TP10 4LL/D = TP10 Leu4→*L/D*-CF_3-Bpg. 20 μM solution of the peptide in 10 mM phosphate buffer was mixed in distinct steps with increasing concentrations of a HS (Sigma-Aldrich, St. Louis, USA, from bovine kidney) stock solution in 10 mM PB. The resulting peptide/HS ratios were in the range of ~ 4:1 down to ~1:25 (mol/mol, where the peptide/HS molar ratio refers to the disaccharide repeating unit of HS). After each addition the mixture was vigorously vortexed and incubated for 30 min at 37°C. Afterwards, spectra of the peptide/HS mixture were recorded at 37°C using a J-815 spectropolarimeter (Jasco, Tokyo, Japan) over the range from 260 to 180 nm at 0.1 nm intervals, using a quartz glass cuvette of 1 mm optical path length (Suprasil, Hellma, Müllheim, Germany), a scan rate of 10 nm/min, 8 s response time and 1 nm bandwidth. Three scans were averaged and the baseline spectrum of the pure phosphate buffer or the corresponding pure HS solution in 10 mM phosphate buffer collected under identical experimental conditions was subtracted. Finally, the baseline-corrected spectra were processed with the adaptive smoothing method, which is part of the Jasco Spectra Analysis software. For calculating the mean residue ellipticity (MRE) spectra the concentration of the fluorophore-labeled peptides was determined by measuring the absorption at 492 nm (maximum of the absorption band of the CF label) in 10 mM phosphate buffer (pH 7.0), assuming a molar extinction coefficient of 75,000 M^{-1} cm^{-1}.

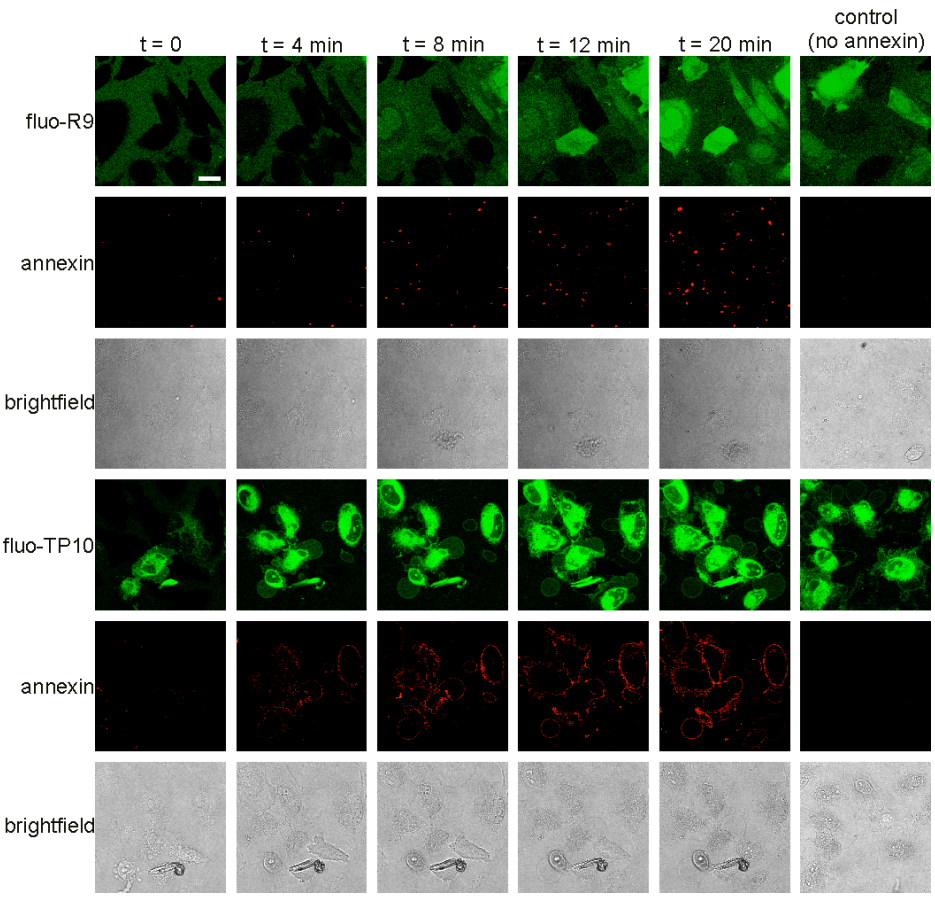


Figure S11. Induction of PS exposure by R9 and TP10. HeLa cells were co-incubated with 25 μM of the indicated peptides and AnnexinV-Alexa Fluor 647. Peptide internalization and PS exposure were followed from the first image acquired (t=0) up to 20 minutes by confocal microscopy. The scale bar corresponds to 20 μm.

[1] T.H. van Kuppevelt, M.A. Dennissen, W.J. van Venrooij, R.M. Hoet, J.H. Veerkamp, Generation and application of type-specific anti-heparan sulfate antibodies using phage display technology. Further evidence for heparan sulfate heterogeneity in the kidney, J Biol.Chem., 273 (1998) 12960-12966.
[2] G.J. Jenniskens, A. Oosterhof, R. Brandwijk, J.H. Veerkamp, T.H. van Kuppevelt, Heparan sulfate heterogeneity in skeletal muscle basal lamina: demonstration by phage display-derived antibodies, J Neurosci, 20 (2000) 4099-4111.
[3] N.C. Smits, A.A. Robbesom, E.M. Versteeg, E.M. van de Westerlo, P.N. Dekhuijzen, T.H. van Kuppevelt, Heterogeneity of heparan sulfates in human lung, Am J Respir Cell Mol Biol, 30 (2004) 166-173.
[4] J.F. Lensen, T.J. Wijnhoven, L.H. Kuik, E.M. Versteeg, T. Hafmans, A.L. Rops, M.S. Pavao, J. van der Vlag, L.P. van den Heuvel, J.H. Berden, T.H. van Kuppevelt, Selection and characterization of a unique phage display-derived antibody against dermatan sulfate, Matrix Biol, 25 (2006) 457-461.

[5] G.B. Ten Dam, S. Yamada, F. Kobayashi, A. Purushothaman, E.M. van de Westerlo, J. Bulten, A. Malmstrom, K. Sugahara, L.F. Massuger, T.H. van Kuppevelt, Dermatan sulfate domains defined by the novel antibody GD3A12, in normal tissues and ovarian adenocarcinomas, Histochem Cell Biol, 132 (2009) 117-127.
[6] T.F. Smetsers, E.M. van de Westerlo, G.B. ten Dam, I.M. Overes, J. Schalkwijk, G.N. van Muijen, T.H. van Kuppevelt, Human single-chain antibodies reactive with native chondroitin sulfate detect chondroitin sulfate alterations in melanoma and psoriasis, J Invest Dermatol, 122 (2004) 707-716.
[7] M.E. Tanner, The enzymes of sialic acid biosynthesis, Bioorganic chemistry, 33 (2005) 216-228.
[8] T. Angata, A. Varki, Chemical diversity in the sialic acids and related alpha-keto acids: an evolutionary perspective, Chem Rev, 102 (2002) 439-469.
[9] A.K. Munster-Kuhnel, J. Tiralongo, S. Krapp, B. Weinhold, V. Ritz-Sedlacek, U. Jacob, R. Gerardy-Schahn, Structure and function of vertebrate CMP-sialic acid synthetases, Glycobiology, 14 (2004) 43R-51R.
[10] J. Dommerholt, S. Schmidt, R. Temming, L.J. Hendriks, F.P. Rutjes, J.C. van Hest, D.J. Lefeber, P. Friedl, F.L. van Delft, Readily accessible bicyclononynes for bioorthogonal labeling and three-dimensional imaging of living cells, Angew Chem Int Ed Engl, 49 (2010) 9422-9425.